Impaired sleep-dependent consolidation after stroke – interaction of slow waves, rehabilitation and GABA

Jaekyung Kim[1,2], Ling Guo[1,2], April Hishinuma[1,2], Stefan Lemke[1,2], Dhakshin S. Ramanathan[1,2#], Seok-Joon Won[1,2*], Karunesh Ganguly[1,2*]

[1] Neurology and Rehabilitation Service, San Francisco Veterans Affairs Medical Center, San Francisco, California, USA.
[2] Department of Neurology, University of California-San Francisco, San Francisco, California, USA.

[#] Current Address: Mental Health Service, VA San Diego Health System, San Diego, San Diego, CA, USA. Department of Psychiatry, University of California, San Diego, San Diego, CA, USA.

* Karunesh Ganguly, MD PhD
1700 Owens Street
San Francisco, CA, 94158, USA
Email karunesh.ganguly@ucsf.edu
* Seok-Joon Won, PhD
1700 Owens Street
San Francisco, CA, 94158, USA
Email seokjoon.won@va.gov

Pages: 36
Figures: 7
Supplementary Figures: 5
Supplementary Tables: 1

ABSTRACT

Sleep is known to be important for promoting recovery after brain injuries such as stroke. Yet, it remains unclear how stroke affects neural processing during sleep and how to precisely enhance sleep-dependent memory consolidation after stroke, i.e., stabilize motor memories during rehabilitation. Using a rat stroke model along with long-term electrophysiological monitoring of neural firing and sleep microarchitecture, here we show that motor memory consolidation after cortical stroke is impaired. Specifically, we find that the precise coupling of spindles to global slow-oscillations (SO), a phenomenon that is known to be important for memory consolidation, is disrupted by a pathological increase in “isolated” local delta waves. The transition from this pathological to a more physiological sleep state – with both a reduction in isolated delta waves and increased spindle coupling to SO – was found to be important for sustained performance gains with task training. Interestingly, post-stroke sleep processing could be pushed towards a more physiological state via a pharmacological reduction of tonic GABA. Together, our results indicate that sleep processing after stroke is impaired due to an increase in local delta waves and that restoration of physiological processing is important for motor memory consolidation during rehabilitation.

KEYWORDS

sleep, stroke, spindles, slow-oscillations, delta-waves, rehabilitation

INTRODUCTION

Stroke is a leading cause of long-term motor disability; despite advancements in acute management and rehabilitation, there are no approved therapies to directly augment neural plasticity (Ganguly et al., 2013; Macdonell et al., 1988; Norrving and Kissela, 2013). Importantly, it is now very clear that a major function of sleep is to regulate neuroplasticity and neural network reorganization (de Vivo et al., 2017; Genzel et al., 2014; Gulati et al., 2017; Gulati et al., 2015; Helfrich et al., 2018; Kim et al., 2019; Klinzing et al., 2019; Krueger et al., 2016; Latchoumane et al., 2017; Ramanathan et al., 2015; Stickgold, 2005; Tononi and Cirelli, 2014; Yang et al., 2014). Thus, optimizing sleep-dependent processing during rehabilitation training has the great potential to enhance recovery. While both clinical and preclinical studies have demonstrated that sleep can influence motor recovery after stroke (Backhaus et al., 2018; Bassetti and Hermann, 2011; Baumann et al., 2006; Duss et al., 2017; Facchin et al., 2020; Gao et al., 2010; Giubilei et al., 1992; Gottselig et al., 2002; Hermann et al., 2008; Poryazova et al., 2015; Siengsukon and Boyd, 2009a; Siengsukon and Boyd, 2009b; Vock et al., 2002), it remains unclear precisely how sleep-dependent processing is affected by stroke.

What might be the features of sleep that are altered by stroke? There is a growing body of literature indicating that the precise coupling of sleep spindles to global slow-waves, i.e., slow-oscillations (SO), is essential for memory consolidation (Born and Feld, 2012; Born et al., 2006; Cairney et al., 2018b; Helfrich et al., 2018; Kim et al., 2019; Latchoumane et al., 2017; Maingret et al., 2016; Ngo et al., 2013). Recent work has also shown that the balance between SO and local slow-waves – delta-waves or δ-waves – determines whether there is effective memory consolidation or, instead, forgetting (Kim et al., 2019). Intriguingly, neurophysiological recordings stroke patients (Poryazova et al., 2015; Sarasso et al., 2020; Tu-Chan et al., 2017; van Dellen et al., 2013) and in animal models (Burns, 1951; Burns and Webb, 1979; Carmichael and Chesselet, 2002; Gulati et al., 2015; Nita et al., 2007) have found a prevalence of *local* low-frequency power (< 4 Hz) during awake periods; this also appears to be far more common after a cortical lesion than a purely subcortical lesion (Macdonell et al., 1988). Together, this might suggest the possibility that post-stroke sleep contains more local δ-waves relative to global SO, thereby perhaps impairing memory consolidation, i.e. bias sleep-dependent processing towards a “forget” state.

Here, we demonstrate that after a cortical stroke, the sleep microarchitecture of the stroke perilesional cortex (PLC) is altered such that there is an imbalance between global SO and local δ-waves. Especially in the early period after stroke, there is an increase in local δ-waves and less effective memory consolidation, i.e. no offline performance gains with task training. With rehabilitation, the sleep microarchitecture slowly became more “reactive”. Thus, with task training, there was a redistribution of sleep spindles towards a more physiological state, characterized by an increase in precise spindle-SO coupling and stronger post-training gains after sleep. Remarkably, this transition could be modulated by a pharmacological treatment that reduced $GABA_A$-mediated tonic inhibition. Together, our results indicate that restoration of physiological sleep processing is important for memory consolidation with rehabilitation training; this allows animals to consolidate each day’s training during long-term rehabilitation and thus allows sustained offline gains in motor performance.

RESULTS

Pathological sleep microarchitecture after stroke: increased local δ-waves

To examine the changes in the temporal interactions of slow waves after cortical stroke, we implanted microelectrode arrays in the PLC (Ramanathan et al., 2018) in two groups of rats (photothrombotic stroke in M1, n = 8 and intact, n = 5; see stroke types and animal groups in Supplementary Table 1). Slow-waves, i.e., SO and δ-waves, were identified using the filtered local field potential (LFP) at 0.1-4 Hz (Fig. 1A). Sleep was detected using video analysis (Pack et al., 2007) and NREM sleep was detected using power spectral density (Supplementary Fig. 1; Methods). We then examined the temporal relationship between δ-waves and SO ($\Delta T_{SO\text{-}\delta}$) (Fig. 1B). In the intact brain, δ-waves typically follow SO; their sequential relation appears to also modulate sleep-dependent processing (Bernardi et al., 2018; Kim et al., 2019; Steriade et al., 1993; Steriade and Timofeev, 2003). We then compared it to the early period after stroke. To specifically identify phases of recovery, we measured motor performance, i.e., pellet retrieval success rate in a reach-to-grasp task (Fig. 1C). The first reach session was often ~1-2 weeks after stroke induction and the reestablishment of food-scheduling (see Methods). Each animal was monitored for 6-10 sessions across 2-3 weeks. Given the variability of recovery times, each animal's sessions were divided into tertiles; each tertile was respectively termed 'early','middle', and 'late'. As expected, the injury resulted in impaired motor performance and there were improvements with subsequent rehabilitation training.

Interestingly, in the early phase after stroke, there was a significant increase in δ-waves that were apparently decoupled from SO, i.e., temporally far from the occurrence of a previous SO. All stroke animals demonstrated this effect compared to healthy animals (Fig. 1D; Supplementary Fig. 2 compares the respective distributions of $\Delta T_{SO\text{-}\delta}$ before and after stroke in the same animal). Using this distribution, we separated δ-waves into two classes, i.e., "SO-coupled/δ_{SO}" and "isolated/δ_I". This distinction was based on simply dividing the $\Delta T_{SO\text{-}\delta}$ distributions using the 50th percentile; δ-waves less than the 50th percentile were labeled δ_{SO}, whereas the remaining δ-waves were labeled δ_I (Methods). Notably, the overall ratios of SO/δ were similar in both stroke and intact animals (stroke: 27.9 ± 2.2%; intact: 32.4 ± 2.6%; stroke vs. intact, two-sample *t*-test, t_{23} = –1.31, P = 0.24). Thus, after stroke, while the relative number of SO and δ-waves were comparable to the intact state, there was a significant increase in the prevalence of local δ_I-waves that were not temporally linked to global SO.

Transition from pathological to physiological sleep processing

For across-session alterations in NREM sleep microarchitecture of the stroke animals, we then examined the changes in the temporal interactions of spindles to SO or δ_I-waves in the PLC. In the intact brain, nesting of spindles to SO has been shown to be important for motor memory consolidation (Antony et al., 2018; Bergmann and Born, 2018; Cairney et al., 2018b; Helfrich et al., 2018; Kim et al., 2019; Latchoumane et al., 2017; Maingret et al., 2016; Ngo et al., 2013; Peyrache et al., 2011; Staresina et al., 2015); moreover, past work has also shown that nesting to local δ-waves has a role in memory forgetting. We thus focused on comparing the nesting of

spindles to SO versus δ_l-waves over the recovery after stroke. For stroke induction, while we used the photothrombotic approach for the data shown in Fig. 1, we also used the endothelin-1 (ET-1) method for three animals (Roome et al., 2014); the ET-1 approach allowed us to collect baseline neural data prior to stroke induction (Methods and below for details). For the ET-1 stroke group, we monitored sleep for 6 session after stroke. The sessions were again evenly divided into early-middle-late phases.

Spindles were detected using the filtered LFP at 10-15 Hz (Fig. 2A; Methods); we then measured nesting of spindles to SO or δ_l-waves in the PLC (Fig. 2B). More specifically, we measured temporal lags between a SO and its nearest spindle ($\Delta T_{SO\text{-}Spindle}$). The "SO-Nesting" focused on the events within –0.5 sec prior to 1 sec after the peak of the up-state; the "δ_l-Nesting" was analyzed in a similar manner, i.e., for δ_l-waves and its closest spindle. With recovery, SO-Nesting became more probable (Fig. 2C) and the distribution of $\Delta T_{SO\text{-}Spindle}$ became sharper, indicating spindles were occurring closer to SO (Fig. 2D). Furthermore, from the distribution of $\Delta T_{SO\text{-}Spindle}$, the SO-Nesting was quantified by the probability of spindles within the nesting window (Fig. 2D gray box, within a –0.5-1s from SO up-states); similar metrics were calculated for δ_l-Nesting. SO-Nesting significantly increased over the period of motor recovery; in contrast, δ_l-Nesting significantly decreased (Fig. 2E). The use of a precise temporal window to define "nesting" meant that this was not simply a consequence of directly shifting spindles from one event to the other. Moreover, there was a strong increase in SO-Nesting and a moderate decrease of δ_l-Nesting in the late period compared to the early period (Fig. 2F). We also examined the rates of SO-nested and δ_l-nested spindles and found a significant increase of the rates in SO-nested spindles (early, n = 22 sessions in 11 rats, 9.9 ± 0.46 count/min vs. late, n = 22 sessions in 11 rats, 11.4 ± 0.56 count/min, mixed-effects model, $t_{42} = 2.15$, P = 0.038; Supplementary Fig. 3). Notably, there was a significant positive relationship between the restoration of SO-Nesting and improvements in the task performance (n = 8 rats in Fig. 1C Pearson's correlation, R = 0.38, P = 0.031), in contrast, there was a negative relationship between changes in δ_l-Nesting and task performance (Pearson's correlation, R = –0.45, $P < 10^{-2}$). The relative nesting, i.e., SO-Nesting/δ_l-Nesting was more predictive of the recovery of task performance (Pearson's correlation, R = 0.48, $P < 10^{-2}$; smaller absolute errors between the true and the predicted performances by SO-Nesting/δ_l-Nesting versus SO-Nesting: paired *t*-test, $t_{31} = 2.18$, P = 0.037). Interestingly, SO-nested spindles were also associated with a significantly stronger spike modulation-depth/MD and amplitudes at the late compared to the early period after stroke (MD, Fig. 2G; amplitude: mixed-effects model, $t_{42} = 2.51$, P = 0.016, Supplementary Fig. 4). Taken together, these results suggest that a change in the precise temporal coupling of spindles toward SO and away from δ_l-waves play a role in functional recovery post-stroke. Moreover, this pathological state was indicative of the *early* post-stroke period, with a transition towards more normal sleep microarchitecture in the *middle-late* period.

Local δ_l-waves preceding SO impedes physiological processing

Is there a more direct relationship of these observed changes in δ_l-waves on SO-spindle nesting? Past studies have shown that changes in SO-associated parameters (e.g., amplitude and refractoriness in spindle generating networks) can depend on the temporal proximity of slow-

waves (Bernardi et al., 2018; Ngo et al., 2015). Given the changes we observed in SO-Nesting with recovery, we thus examined whether changes in how often δ_l-waves directly preceded a SO event could predict this change. We specifically examined how many δ_l-waves preceded SO, i.e., –5-0s from a SO up-state (Fig. 3A). Remarkably, this phenomenon appeared to significantly influence spindle nesting to SO; we found a strong negative correlation between the δ_l-wave rate preceding SO and SO-Nesting (Fig. 3B). Thus, our results suggest that the prevalence of δ_l-waves in the early stroke may directly impede the nesting of spindles to SO and influence motor recovery after stroke.

Transition to physiological sleep enhanced task-specific rehabilitation

As described above, we found that the redistribution of spindles toward SO and away from δ_l-waves could account for long-term across-session recovery, i.e., over a ~3 weeks period after stroke. We also wondered whether the nesting of spindles was modulated by rehabilitation training after stroke, i.e., short-term *within-session* daily effects of the training. Notably, numerous studies have shown that during NREM sleep after training, SO, spindles, and their precise temporal interaction play a role in offline memory consolidation in the intact brain (Bergmann and Born, 2018; Cairney et al., 2018b; Diekelmann and Born, 2010; Genzel et al., 2014; Helfrich et al., 2018; Kim et al., 2019; Latchoumane et al., 2017; Maingret et al., 2016; Miyamoto et al., 2017; Navarro-Lobato and Genzel, 2019; Ngo et al., 2013; Peyrache et al., 2009; Sejnowski and Destexhe, 2000; Silversmith et al., 2020; Staresina et al., 2015). Interestingly, while SO-Nesting increased when comparing the pre- to post-training sleep in the early and late priods, δ_l-Nesting significantly decreased in the post-training sleep in the corresponding period (Fig. 4B). There was not a change in the rate of SO-nested and δ_l-nested spindles (early vs. late, ΔSO-nested: mixed-effects model, $t_{30} = 1.27$, $P = 0.21$; $\Delta\delta_l$-nested: mixed-effects model, $t_{30} = -1.34$, $P = 0.19$; Supplementary Fig. 5). Furthermore, the changes in SO-Nesting relative to the changes in δ_l-Nesting was associated with changes in task-performance the following day (Fig. 4C). In other words, with continued time after stroke, rehabilitation training appeared to be able to trigger reactive changes in the subsequent sleep period; this appeared to manifest as improved performance the following day.

Does sleep duration benefit recovery when sleep after stroke is in a more physiological state? We thus specifically assessed the effects of sleep duration on recovery in animals that were in the *midddle-late phase* of recovery post-stroke*;* this was defined by the period in which each animal first demonstrated performance improvements. In other words, we did not use *early stroke* periods when the animals showed static deficits; as shown above, this period was linked to abnormal sleep reactivity. Thus, in a separate group of photothrombotic stroke animals, we measured the effects of sleep on the subsequent task and compared this to a sleep restriction group. We measured the duration of sleep using video-based detection methods (n = 29 sessions in 6 rats). In the restriction group (n = 28 sessions in 8 rats), sleep was deprived either 2 or 6 hours after the training session and then the retrieval session was conducted (n = 4 restricted 2 hours; n = 4 restricted 6 hours). The rats with post-training sleep experienced greater offline gains in comparison to the sleep-restricted animals (Fig. 5A). We also found a significant relationship between sleep duration and changes in task performance using the middle-late period (Fig. 5B);

however, there was no significant relationship with sleep duration when considering the early and middle phases of recovery (linear regression, R = 0.278, P = 0.15). We interpreted these results to mean that sleep duration was specifically beneficial during the middle-late period of recovery. It also suggests that sleep-dependent processing during recovery relies on reestablishment of physiological sleep architecture.

Reducing elevated tonic inhibition and pathological sleep

What might be the underlying neurophysiological basis for our observed changes in SO and δ_l-waves with recovery? While changes in structural connectivity over time might contribute, another intriguing possibility is that known post-stroke elevations in extra-synaptic γ-aminobutyric acid (GABA) may perturb the ability of global SO to organize local δ-waves. Studies have reported that elevated $GABA_A$-mediated tonic inhibition reduces network excitability, and that reducing such inhibition can have a beneficial effect on recovery (Clarkson et al., 2010; He et al., 2019). These studies specifically imply that an altered excitation-inhibition balance (Kim and Fiorillo, 2017; Xia et al., 2017; Yizhar et al., 2011) plays an important role in motor recovery. Thus, we tested the effects of blocking $GABA_A$-mediated tonic inhibition after stroke on the temporal coupling of spindles to slow-waves. We specifically assessed the effects of injecting $GABA_A$ α5-subtype receptor inverse agonist (L655-708) (Clarkson et al., 2010) during early recovery after a photothrombotic stroke (n = 3 animals) and an ET-1 induced stroke (n = 3 animals); for the ET-1 induced stroke microelectrode arrays targeted to PLC with an attached cannula were used for infusion of ET-1 into M1 (Methods). Baseline spiking/LFP activity was recorded before inducing stroke; this was followed by recordings after the injection of vehicle (sham) or L655-708 (drug) during the early stroke, i.e., days 7~12 after stroke (Fig. 6A).

Strikingly, the treatment with the drug resulted in significantly stronger SO-spindle nesting with a concomitant reduction in δ_l-spindle nesting (Fig. 6B). We observed increased excitability when comparing the drug versus the sham conditions. For example, the modulation-depth of cortical spiking during SO was stronger with the treatment condition (Fig. 6C). Moreover, changes in the modulation-depth of cortical spiking during spindles, a measure of the effectiveness of spindles in modulating local spiking, could be explained by both an increase in SO-nesting (Fig. 6D). Thus, our results indicate that elevated $GABA_A$-mediated tonic inhibition can partially account for the altered sleep microarchitecture in the early stroke period.

DISCUSSION

Overall, our results reveal how sleep processing is affected by stroke and how such processing interacts with task training during rehabilitation (Fig. 7). First, our results indicate that, after stroke, the sleep microarchitecture is dominated by local δ_l-waves that impeded the beneficial effects of SO-spindle nesting on motor memory consolidation. Transition to more normal sleep processing was found to be important for realizing the benefits of rehabilitation. Second, our results link changes in extracellular tonic GABA to the pathological sleep state after stroke. We also show that existing pharmacological therapies might offer a path to normalizing abnormal sleep processing after stroke. Third, we provide a direct link between rehabilitation training during recovery to "reactive" SO-spindle nesting changes in sleep; this may be a key driver of consolidation and offline gains. Together, our results offer a roadmap to delineate normal vs pathological sleep after stroke and offer novel therapeutic targets (e.g., tonic GABA and SO-spindle nesting) to modulate sleep in order to enhance recovery after stroke.

EEG studies in stroke patients (Macdonell et al., 1988; Poryazova et al., 2015; Tu-Chan et al., 2017; van Dellen et al., 2013) and LFP recordings in animal models (Carmichael and Chesselet, 2002; Gulati et al., 2015) have found evidence of increased low-frequency power during awake periods after stroke. These studies have also indicated that this increased awake low-frequency power is a marker of cortical injury and loss of subcortical inputs post-stroke (Topolnik et al., 2003). Our findings of increased local δ_l-waves during post-stroke sleep are perhaps related to this phenomenon. Importantly, the increased frequency of δ_l-waves preceding SO was closely associated with the attenuated temporal coupling of spindles to SO (Fig. 3B); the normalization of SO-δ_l interactions towards a physiological state with recovery drove more precise coupling of spindles and, therefore, performance gains. There is also growing evidence that the temporal coupling of spindles to SO are essential drivers of memory consolidation during sleep (Antony et al., 2018; Cairney et al., 2018b; Helfrich et al., 2018; Kim et al., 2019; Latchoumane et al., 2017; Maingret et al., 2016; Staresina et al., 2015). Such coupling has been linked to spike-time dependent plasticity (Bergmann and Born, 2018). It is also a potent driver of the reactivation of awake experiences (Antony et al., 2018; Cairney et al., 2018a; Ngo et al., 2013; Peyrache et al., 2009). Finally, disruption of this coupling has been found to impair memory consolidation after awake experiences (Kim et al., 2019). Thus, our results link pathological changes in network physiology after stroke to impaired sleep-dependent processing, primarily via a disruption in the precise spindle-SO coupling.

Changes in sleep-dependent processing after stroke were found to closely interact with rehabilitation training during the preceding awake period. At present, such training is the mainstay of treatment after acquired brain injuries after stroke (Bernhardt et al., 2017; Ganguly et al., 2013; Pearson-Fuhrhop et al., 2009). Our results specifically indicate that marking whether sleep is in a pathological state or physiological state may be an important consideration for the timing of intense rehabilitation. Our current results do not allow us to determine whether this transition is specifically an early benefit of attempted rehabilitation or a process that is independent of training. Past studies in rodents have suggested a critical period in which training can trigger long-term benefits (Dromerick et al., 2009; Krakauer et al., 2012). Notably, if its indeed the case that awake low-frequency power in stroke patients is related to our observed effects on sleep processing, it might help explain past results indicating that awake low-frequency power is a predictor of recovery. Future studies using EEG can measure in greater detail how changes in the coupling

of spindles to SO and δ_I-waves predict the benefits of task training. Such studies can also help delineate when and if the transition to physiological sleep occurs; this is particularly important as the time course of recovery is much longer in humans than in rodents.

Our results also have implications for future translational studies. Animal studies have suggested that $GABA_A$-mediated tonic inhibition in the PLC may be a therapeutic target to promote recovery in the acute phase of stroke; blockade of $GABA_A$-mediated tonic inhibition was found to promote stroke recovery (Clarkson et al., 2010; He et al., 2019). Both short-term (i.e., acutely prior to task training) and long-term (i.e., chronic infusion) of the drug have been tested. Intriguingly, long-term infusion appears to be much better (Clarkson et al., 2010). Our results provide a possible mechanism for why long-term infusion may be essential to achieve prominent benefits; more specifically, the effect of this drug might not only help with task-specific online training but also promote offline memory consolidation during sleep. Such knowledge is likely to be critical for successful translation to clinical populations. It is also quite likely that SO and local δ-waves can be monitored using non-invasive EEG recording in clinical stroke patients, ideally allowing patient-specific therapeutics. For example, non-invasive brain stimulation during sleep on memory consolidation (Antony et al., 2018; Cairney et al., 2018b; Ngo et al., 2013) can be tailored based on suppressing local delta waves or enhancing SO.

In conclusion, our results reveal that in the early stroke period, there are increased pathological isolated δ_I-waves that appear to impede memory consolidation by altering physiological coupling to spindles; elevated tonic GABA inhibition is a key mediator of this pathological state. In a more normal physiological sleep state, we observed allows for reactive increases in the precise temporal nesting of spindles to SO. This is likely to be very important for promoting motor memory consolidation and improved long-term recovery with neurorehabilitation.

METHODS

Animals/surgery

Experiments were approved by the Institutional Animal Care and Use Committee at the San Francisco VA Medical Center. We used a total of twenty-five adult Long-Evans male rats; twenty-three rats with stroke and two rats without stroke (Supplementary Table 1; detailed contributions of each rat on the respective results). No statistical methods were used to pre-determine sample sizes, but our sample sizes are similar to those reported in previous publications (Gulati et al., 2017; Gulati et al., 2014; Ramanathan et al., 2015). Animals were kept under controlled temperature and a 12-h light: 12-h dark cycle with lights on at 06:00 a.m. Surgeries were performed under isofluorane (1-3%) anesthesia and body temperature was maintained at 37 °C with a heating pad. Atropine sulfate was also administered before anesthesia (0.02 mg/kg of body weight). We implanted 32/128-channel microwire arrays for recording LFP/spike activity; arrays were lowered down to 1,400-1,800 μm in the layer 5 of the primary motor cortex (M1) or prelesional cortex (PLC) in the upper limb area (1-3 mm anterior to bregma and 2-4 mm lateral from midline). The reference wire was wrapped around a screw inserted in the midline over the cerebellum. Final localization of depth was based on quality of recordings across the array at the time of implantation. The post-operative recovery regimen included administration of buprenorphine at 0.02 mg/kg and meloxicam at 0.2 mg/kg. Dexamethasone at 0.5 mg/kg and Trimethoprim sulfadiazine at 15 mg/kg were also administered post-operatively for 5 days. All animals were allowed to recover for at least five days with the same regimen as described above before start of experiments. Data collection and analysis were not performed blind to the conditions of the experiments.

Photothrombotic and endothelin-1 induced focal stroke

We used either photothrombotic and Endothelin-1 (ET-1) induced stroke models (see stroke types for each group of animals in Supplementary Table 1). For the photothrombotic stroke, rose bengal dye was injected into the femoral vein using and intravenous catheter after craniotomy. Next, the surface of the brain was illuminated with white light (KL-1500 LCD, Schott) using a fiber optic cable for 20 min. We used a 4-mm aperture for stroke induction (centered in the M1 area based on stereotactic coordinates) and covered the remaining cortical area with a custom aluminum foil mask to prevent light penetration. After induction, a probe was implanted in the PLC immediately anterior to the stroke site (Gulati et al., 2015; Ramanathan et al., 2018). The craniotomy or implanted electrodes were covered with a layer of silicone (Quiksil), followed by dental cement. For the precise measure of baseline LFP/spike activity before inducing stroke, we also used ET-1 induced focal stroke model (Robinson et al., 1990; Roome et al., 2014; Sharkey et al., 1993; Virley et al., 2004) in three rats (Fig. 6). Microarray attached with infusion cannula (guide: 26G; internal: 33G; P1 Technology) was implanted into the M1 area; single cannula in one rat and bilateral cannula with 2 mm spacing in the other two rats. The remaining operation procedure was same as the photothrombotic stroke. The ET-1 induced stroke allowed us to induce the focal stroke following a baseline measurement; after measuring baseline activity, ET-1 was injected with 1.5 ul through single cannula in one rat and total 2.0 ul (1.0 ul for each) through bilateral cannula (100 nl per min) in the other two rats into deep cortical layers (1.4 mm from surface of brain).

375 **Electrophysiology**

376 We conducted AC-coupled recordings and recorded extracellular neural activity using 32-channel
377 microwire electrode arrays (MEAs; 33-μm-length, 250-μm-spacing, 4-rows, standard polyimide-
378 coated tungsten microwire arrays from Tucker-Davis Technologies (TDT) for six rats; 25-μm-
379 length, 200-μm-spacing, 6-rows, tungsten microwire arrays from Innovative Neurophysiology Inc.
380 for 5 rats) and 128-channel custom electrode arrays (Egert D, 2018) (for 1 rat). We recorded
381 spike and LFP activity using a 128-channel RZ2 bioamp processor (TDT) and 128-channel
382 neurodigitizer (digital PZ4 and PZ5).

383 Spike data was sampled at 24,414 Hz and LFP data at 1,018 Hz. ZIF-clip-based headstages
384 (TDT) for 32-channel microwires and SPI-based headstates (Intan Technologies) for 128-channel
385 microwire with a unity gain and high impedance (~1 G) was used. Only clearly identifiable units
386 with good waveforms and high signal-to-noise ratio were used. The remaining neural data (e.g.
387 filtered LFP) was recorded for offline analysis at 1,018 Hz. Behavior related timestamps (that is,
388 trial onset and trial completion) were sent to the RZ2 analog input channel using a digital board
389 and synchronized to neural data. Electrophysiology was not monitored during the baseline
390 sessions in eight rats and during all sessions in twelve rats (Supplementary Table 1).

391

392 **Behavior**

393 After recovery, animals were typically handled for several days before the start of experimental
394 sessions. Animals were acclimated to a custom plexiglass behavioral box (Fig. 4A) during this
395 period. The box was equipped with a door at one end. In three rats (ET-1 stroke), animals
396 experienced spontaneous recovery without rehabilitation training. In the other twenty-two rats,
397 animals were trained to a plateau level of performance in a reach-to-grasp single-pellet task
398 before neural probe implantation or photothrombotic stroke induction. Probe implantation and
399 stroke induction was performed contralateral to the preferred hand. Animals were allowed to rest
400 at least for 5 days before the start of experimental or recording sessions post-stroke. For the
401 photothrombotic stroke group, animals experienced rehabilitation training until reaching a plateau
402 level of performance (Fig. 1C). The first reach session for the "across-session" analyses was
403 often ~1-2 weeks because of food-scheduling and the ability to start trials. Each animal was
404 monitored for 6 – 10 session until a plateau was reached. Given the variability of recovery times,
405 and as described in the results, sessions per animal were divided into tertiles and termed 'early',
406 'middle' and 'late'. During behavioral assessments, we monitored the animals and ensured that
407 their body weights did not drop below 90% of their initial weight.

408 We used an automated reach-box, controlled by custom MATLAB scripts and an Arduino
409 microcontroller. This setup required minimal user intervention, as described previously (Wong et
410 al., 2015). Each trial consisted of a pellet dispensed on the pellet tray, followed by an alerting
411 beep indicating that the trial was beginning and then the door opening. Animals then had to reach
412 their arm out, grasp and retrieve the pellet. A real-time "pellet detector" using an infrared detector
413 centered over the pellet was used to determine when the pellet was moved, which indicated that
414 the trial was over and the door was closed. All trials were captured by video, which was synced
415 with the electrophysiology data using Arduino digital output. The video frame rate was 30 Hz for
416 the six animals and 75 Hz sixteen animals. The task performance (the number of accurate pellet
417 retrieval/the total number of trial x 100 %) was determined manually from a recorded video.

418

419 **$GABA_A$ α5-subtype receptor inverse agonist treatment**

420 The treatment with $GABA_A$ α5-subtype receptor inverse agonist (L655,708; "drug" condition in Fig.
421 6) was initiated with delayed period (7 days) after ET-1 induced stroke; the previous studies
422 reported the effect of L655,708 promoted functional recovery 7 days after stroke (Clarkson et al.,
423 2010; He et al., 2019). At the time 0.5~1 hour before the beginning of sleep, rats received
424 intraperitoneal injections of vehicle (i.e., saline; "sham" condition) or L655,708 (Sigma-Aldrich; 5
425 mg/kg, dissolved in dimethylsulphoxide/DMSO and then diluted 1:1 in 0.9% saline) once daily for
426 6 consecutive days; sham or drug was operated every other day at days 7~12 after stroke to
427 examine the effect of L655,708 in LFP/spike activity.

428

429 **Analyses across-session versus within-session**

430 Animals typically experienced rehabilitation reaching task during the recovery period; in sequence,
431 pre-training sleep, Reach1 training, post-training sleep, and Reach2 retrieval with a single-day
432 session (Fig. 4A) except three animals that experienced only spontaneous recovery. In Figs. 1,
433 2, and 3, we specifically analyzed the pre-training sleep and the Reach1 training in
434 photothrombotic stroke animals; for the ET-1 animals we focused on spontaneous changes in
435 sleep microarchitectures without rehabilitation over a ~3 recovery period. These two analyses
436 are hereafter termed "across-session" analysis. In the animals that experienced reach-to-grasp
437 single-pellet task, the sessions prior to reaching a plateau level of performance were analyzed.
438 In each animal, the 1-2 weeks recovery period was divided into sextiles and a representative
439 session in each sextile was used. In Figs. 4 and 5, we compared sleep metrics and task
440 performances within a single-day experiment (i.e., "within-session" analyses). Sleep metrics (e.g.,
441 SO-Nesting and δ_l-Nesting) were measured in a pair of pre-training and post-training sleep in a
442 single-day session, then the change from the pre-training to the post-training sleep was computed
443 (e.g., ΔSO-Nesting and $\Delta\delta_l$-Nesting, respectively). Task performances were also compared the
444 same way from Reach1 training to Reach2 retrieval (i.e., ΔTask performance).

445

446 **Identification of NREM sleep waves**

447 The LFP activity was recorded using 32/128-channel microwire electrode arrays (see above).
448 The LFP was analyzed after removing obvious artifacts and excluding bad channels.
449 Identification of NREM epochs was performed by classification based on power spectral density
450 of LFP. LFP trace was segmented into non-overlapping 6 sec epochs. In each epoch the power
451 spectral density was computed and averaged over the SO/δ (0.1-4 Hz) and gamma (30-60 Hz)
452 frequency bands. Then a k-means classifier was used to classify epochs into two clusters, NREM
453 sleep and REM/awake. Sleep epochs less than 30 sec were excluded from NREM sleep epochs.
454 The identified NREM sleep durations were not different between early period and late period of
455 stroke (Supplementary Fig. 1B). The identified NREM sleep epochs were verified by visual
456 assessment of the LFP activity. This power-based sleep detections showed a close match to the
457 video-based detections (Pack et al., 2007) (Supplementary Fig. 1A); the number of pixels which
458 change intensity frame to frame in each pair of consecutive frames was computed from a recorded
459 video during sleep block and then integrated those number of pixels during an epoch of 40 sec.

If that integrated value was higher than threshold, that epoch was identified as sleep; the threshold was chosen by comparing detection results and visual assessment of the recorded video. In Fig. 5, sleep duration during post-training sleep was detected by video-based assessment (see above Methods). We then used this to predict performance changes from Reach1 to Reach2 for the sleep group; in the no-sleep group, moderate vibration on the behavior box was given when the rats were not active for > 40 sec, to prevent from sleeping.

In offline analysis, SO, δ-waves and spindles were detected using the algorithm used in the previous study (Kim et al., 2019). The LFP average across all recording channels excluding bad channels was filtered in the SO/δ band (0.1-4 Hz) through two independent filtering; the high pass Butterworth filter (2nd order, zero phase shifted, with a cutoff at 0.1 Hz) was applied and then followed by the low pass Butterworth filter (5th order, zero phase shifted, with a cutoff at 4 Hz). Next, all positive-to-negative zero crossings during NREM sleep were identified, along with the previous peaks, the following troughs, and the surround negative-to-positive zero crossings. Then the positive threshold (the top 15 percentile of the peaks) and the negative threshold (the bottom 40 percentile of the troughs) were respectively defined for the down-states and up-states. Each identified wave was considered a SO if the trough was lower than the negative threshold (i.e., up-state), the peak preceding that up-state was higher than the positive threshold (i.e., down-state), and the duration between the peak and the trough was between 150 ms and 500 ms (Fig. 1A). On the other hand, a slow wave was considered a δ-wave if the trough was lower than the negative threshold (i.e., up-states) and that the up-state was preceded by maximum voltage that was lower than the positive threshold within 500 ms. In this study we separated δ-waves into two classes depending on their temporal interaction with a preceding SO, i.e., $\Delta T_{SO\text{-}\delta}$ (Fig. 1B and D). $\Delta T_{SO\text{-}\delta}$ > 100 sec (1~2%) were manually removed to exclude the cases driven by the possible error in NREM sleep detections; this error was evaluated by visual inspection of slow-wave activity. From the distribution of $\Delta T_{SO\text{-}\delta}$ in intact brains (n = 9 sessions, 5 rats), 50th percentile of $\Delta T_{SO\text{-}\delta}$ (3.7 sec) was set as the cutoff separating δ-waves into "SO-coupled δ/δ_{SO}" and "isolated δ/δ_I" waves; δ-waves within the close 50% from a preceding SO ($\Delta T_{SO\text{-}\delta} \leq 3.7$ sce) were labeled "δ_{SO}," whereas δ-waves of the distal 50% from a preceding SO ($\Delta T_{SO\text{-}\delta} > 3.7$ sce) were labeled "δ_I." The cutoff of $\Delta T_{SO\text{-}\delta}$ determined by intact conditions was also used for stroke conditions.

For spindle detection, the LFP was first z-scored in each channel and averaged across all good channels. The LFP average was filtered in spindle band (10-15 Hz) through two independent filtering (Fig. 2A); the high pass Butterworth filter (6th order, zero phase shifted, with a cutoff at 10 Hz) was applied and then followed by the low pass Butterworth filter (8th order, zero phase shifted, with a cutoff at 15 Hz). We computed a smoothed envelope of this signal, the magnitude of the Hilbert transforms with convolving by a Gaussian window (200 ms). Next, we determined two thresholds for spindle detection based on the mean (μ) and standard deviation (σ) of the spindle band LFP during NREM sleep; the upper and lower thresholds were set $\mu + 2.5 \times \sigma$ and $\mu + 1.5 \times \sigma$, respectively. Epochs in which the spindle power exceeded the upper threshold for at least one sample and the spindle power exceeded the lower threshold for at least 500 ms were considered spindles. Each epoch where the spindle power exceeded the lower threshold was considered the start and stop of the spindle; the duration of each spindle was based on these values as well.

Spindle nesting analyses

We also analyzed the temporal coupling of spindles relative to SO or δ-waves. For the nesting of spindles to SO (SO-Nesting; Fig. 2B left), each spindle was linked to the closest SO. The time difference between the peak of spindle and the up-state of the linked SO was measured for each detected spindle ($\Delta T_{SO\text{-}Spindle}$). If $\Delta T_{SO\text{-}Spindle}$ was between –0.5 sec and 1.0 sec (i.e., nesting time window), that spindle event was considered a SO-nested spindle. In this study, we focused on the temporal interaction of spindles to the δ_l-waves. Thus, the nesting of spindles to δ_l (δ_l-Nesting; Fig. 2B right) was identified in a manner analogous to the "SO-Nesting" value, i.e., time differences between the spindle peak time and the time of the δ_l up-state. To quantitatively assess the changes in temporal coupling of spindles to SO, we specifically measured as the following; time lag of spindle from the closest SO ($\Delta T_{SO\text{-}Spindle}$) was measured for each spindle event and the rate of spindles of which $\Delta T_{SO\text{-}Spindle}$ was within the nesting time window was measured; i.e., the number of SO-nested spindles / the total number of spindles × 100 % (Fig. 2C and D). We also measured δ_l-Nesting the same way as the "SO-Nesting" but using time lags between the peaks of spindles and the up-states of the linked δ_l; i.e., the number of δ_l-nested spindles / the total number of spindles × 100 %.

Spike activity during sleep waves

We initially used an online sorting program (SpikePac, TDT). We then conducted offline sorting using Plexon Inc's Offline Sorter. Only clearly identifiable units with good waveforms and high signal-to-noise ratio were used. After spikes were time locked to events reference time (SO up-states and SO-nested spindles), the peri-event time histogram (PETH, bin length 20 ms) was estimated. Then, unit modulation-depth (MD) was calculated by comparing the difference between maximum and minimum around events time (within –0.5 to 0.3 sec from SO up-states and –0.25 to 0.15 sec from spindles peaks) over the baseline firing activity (averaged activity within –2 to –0.5 sec from the events); i.e., (maximum – minimum)/baseline firing rate. In other words, the MD is a measure of the modulation of firing rate relative to the pre-event start baseline rate. This was compared for early period and late period of stroke in Fig. 2G and for the sham and drug conditions in Fig. 6C and D. No significant change in population spike rates was found from early to late period (Supplementary Fig. 4A).

Quantification and statistical analyses

Figures show mean ± s.e.m.; if this was not case, we specifically indicated it. Parametric statistics were generally used in this study (linear mixed-effect model, *t*-tests, linear regression, Pearson's correlation otherwise stated); they were implemented within MATLAB. The linear mixed-effects model (using MATLAB "fitlme") was used to compare the differences in task performance, temporal coupling of spindles to SO, and reactivation strength. This model accounts for the fact that units, channels, events, or trials from the same animal are more correlated than those from different animals and is more stringent than computing statistical significance over all units, channels, events, and trials (Aarts et al., 2014). We fitted random intercepts for each rat and reported the P values for the regression coefficients associated with stroke versus intact conditions, early period versus late period stroke, sham versus drug, and sleep versus no-sleep. The used random effects and fixed effects parameters are following; Figs. 2G, H and 4B and Supplementary Figs. 1B, 3 right, 4, and 5, random: rat, fixed: stroke period; Fig. 5A, random: rat, fixed: sleep type; Fig. 6B and C, random: rat, fixed: injection type. In these figures, mean in each

experiment session was used as the response parameter. Regression modeling for fixed-effects provide intercept and slope in mixed-effects model comparison.

For the comparison between distributions we used Kolmogorov-Smirnov's test in Fig. 1D and Supplementary Fig. 2 to test the samples were drawn from the same distribution and Bartlett's test in Fig. 2D to test equal variances (sharpness of distribution) between early period and late period stroke. We used linear regression or correlation to evaluate the relationship between the recovery period and the sleep metrics (e.g. SO-Nesting and δ_l-Nesting) in Fig. 2E and Supplementary Fig. 3 left; between the mean rate of δ_l preceding SO and the SO-Nesting in Fig. 3B; between the changes in SO/δ_l-Nesting and the next-day task performance in Fig. 4C; between the post-training sleep duration and the changes in task performance in Fig. 5B; between the changes of SO-Nesting and the changes in spindles-MD in Fig. 6D.

REFERENCES

Aarts, E., Verhage, M., Veenvliet, J.V., Dolan, C.V., and van der Sluis, S. (2014). A solution to dependency: using multilevel analysis to accommodate nested data. Nature neuroscience *17*, 491-496.

Antony, J.W., Piloto, L., Wang, M., Pacheco, P., Norman, K.A., and Paller, K.A. (2018). Sleep Spindle Refractoriness Segregates Periods of Memory Reactivation. Curr Biol *28*, 1736-1743 e1734.

Backhaus, W., Braass, H., Gerloff, C., and Hummel, F.C. (2018). Can Daytime Napping Assist the Process of Skills Acquisition After Stroke? Frontiers in neurology *9*, 1002.

Bassetti, C.L., and Hermann, D.M. (2011). Sleep and stroke. In Handbook of clinical neurology (Elsevier), pp. 1051-1072.

Baumann, C.R., Kilic, E., Petit, B., Werth, E., Hermann, D.M., Tafti, M., and Bassetti, C.L. (2006). Sleep EEG changes after middle cerebral artery infarcts in mice: different effects of striatal and cortical lesions. Sleep *29*, 1339-1344.

Bergmann, T.O., and Born, J. (2018). Phase-Amplitude Coupling: A General Mechanism for Memory Processing and Synaptic Plasticity? Neuron *97*, 10-13.

Bernardi, G., Siclari, F., Handjaras, G., Riedner, B.A., and Tononi, G. (2018). Local and Widespread Slow Waves in Stable NREM Sleep: Evidence for Distinct Regulation Mechanisms. Front Hum Neurosci *12*, 248.

Bernhardt, J., Hayward, K.S., Kwakkel, G., Ward, N.S., Wolf, S.L., Borschmann, K., Krakauer, J.W., Boyd, L.A., Carmichael, S.T., and Corbett, D. (2017). Agreed definitions and a shared vision for new standards in stroke recovery research: the stroke recovery and rehabilitation roundtable taskforce. International Journal of Stroke *12*, 444-450.

Born, J., and Feld, G.B. (2012). Sleep to upscale, sleep to downscale: balancing homeostasis and plasticity. Neuron *75*, 933-935.

Born, J., Rasch, B., and Gais, S. (2006). Sleep to remember. Neuroscientist *12*, 410-424.

Burns, B.D. (1951). Some properties of isolated cerebral cortex in the unanaesthetized cat. The Journal of physiology *112*, 156.

Burns, B.D., and Webb, A.C. (1979). The correlation between discharge times of neighbouring neurons in isolated cerebral cortex. Proceedings of the Royal Society of London Series B Biological Sciences *203*, 347-360.

Cairney, S.A., Guttesen, A.A.V., El Marj, N., and Staresina, B.P. (2018a). Memory Consolidation Is Linked to Spindle-Mediated Information Processing during Sleep. Curr Biol *28*, 948-954 e944.

Cairney, S.A., Guttesen, A.A.V., El Marj, N., and Staresina, B.P. (2018b). Memory Consolidation Is Linked to Spindle-Mediated Information Processing during Sleep. Current Biology *28*, 948-954.

Carmichael, S.T., and Chesselet, M.F. (2002). Synchronous neuronal activity is a signal for axonal sprouting after cortical lesions in the adult. Journal of Neuroscience *22*, 6062-6070.

596 Clarkson, A.N., Huang, B.S., Macisaac, S.E., Mody, I., and Carmichael, S.T. (2010). Reducing
597 excessive GABA-mediated tonic inhibition promotes functional recovery after stroke. Nature *468*,
598 305-309.

599 de Vivo, L., Bellesi, M., Marshall, W., Bushong, E.A., Ellisman, M.H., Tononi, G., and Cirelli, C.
600 (2017). Ultrastructural evidence for synaptic scaling across the wake/sleep cycle. Science *355*,
601 507-510.

602 Diekelmann, S., and Born, J. (2010). The memory function of sleep. Nat Rev Neurosci *11*, 114-
603 126.

604 Dromerick, A.W., Lang, C.E., Birkenmeier, R.L., Wagner, J.M., Miller, J.P., Videen, T.O., Powers,
605 W.J., Wolf, S.L., and Edwards, D.F. (2009). Very Early Constraint-Induced Movement during
606 Stroke Rehabilitation (VECTORS) A single-center RCT. Neurology *73*, 195-201.

607 Duss, S.B., Seiler, A., Schmidt, M.H., Pace, M., Adamantidis, A., Muri, R.M., and Bassetti, C.L.
608 (2017). The role of sleep in recovery following ischemic stroke: A review of human and animal
609 data. Neurobiol Sleep Circadian Rhythms *2*, 94-105.

610 Egert D, P.J., Batmutsky I, Caldwell CM, Roossien J, Patel PR, Lemke S, Ganguly K, Cai D,
611 Chestek CA, Berke JD (2018). Cellular-scale probes for high-density, precisely-localized
612 neurophysiology. Paper presented at: Society for Neuroscience Annual Meeting: available at
613 https://wwwabstractsonlinecom/pp8/#!/4649/presentation/24873.

614 Facchin, L., Schone, C., Mensen, A., Bandarabadi, M., Pilotto, F., Saxena, S., Libourel, P.A.,
615 Bassetti, C.L.A., and Adamantidis, A.R. (2020). Slow Waves Promote Sleep-Dependent Plasticity
616 and Functional Recovery after Stroke. The Journal of neuroscience : the official journal of the
617 Society for Neuroscience *40*, 8637-8651.

618 Ganguly, K., Byl, N.N., and Abrams, G.M. (2013). Neurorehabilitation: Motor Recovery After
619 Stroke as an Example. Annals of Neurology *74*, 373-381.

620 Gao, B., Cam, E., Jaeger, H., Zunzunegui, C., Sarnthein, J., and Bassetti, C.L. (2010). Sleep
621 disruption aggravates focal cerebral ischemia in the rat. Sleep *33*, 879-887.

622 Genzel, L., Kroes, M.C., Dresler, M., and Battaglia, F.P. (2014). Light sleep versus slow wave
623 sleep in memory consolidation: a question of global versus local processes? Trends in
624 neurosciences *37*, 10-19.

625 Giubilei, F., Iannilli, M., Vitale, A., Pierallini, A., Sacchetti, M., Antonini, G., and Fieschi, C. (1992).
626 Sleep patterns in acute ischemic stroke. Acta neurologica scandinavica *86*, 567-571.

627 Gottselig, J.M., Bassetti, C.L., and Achermann, P. (2002). Power and coherence of sleep spindle
628 frequency activity following hemispheric stroke. Brain : a journal of neurology *125*, 373-383.

629 Gulati, T., Guo, L., Ramanathan, D.S., Bodepudi, A., and Ganguly, K. (2017). Neural reactivations
630 during sleep determine network credit assignment. Nature neuroscience *20*, 1277-1284.

631 Gulati, T., Ramanathan, D.S., Wong, C.C., and Ganguly, K. (2014). Reactivation of emergent
632 task-related ensembles during slow-wave sleep after neuroprosthetic learning. Nature
633 neuroscience *17*, 1107-1113.

634 Gulati, T., Won, S.J., Ramanathan, D.S., Wong, C.C., Bodepudi, A., Swanson, R.A., and Ganguly,
635 K. (2015). Robust neuroprosthetic control from the stroke perilesional cortex. The Journal of
636 neuroscience : the official journal of the Society for Neuroscience *35*, 8653-8661.

637 He, W.M., Ying-Fu, L., Wang, H., and Peng, Y.P. (2019). Delayed treatment of alpha5 GABAA
638 receptor inverse agonist improves functional recovery by enhancing neurogenesis after cerebral
639 ischemia-reperfusion injury in rat MCAO model. Sci Rep *9*, 2287.

640 Helfrich, R.F., Mander, B.A., Jagust, W.J., Knight, R.T., and Walker, M.P. (2018). Old Brains
641 Come Uncoupled in Sleep: Slow Wave-Spindle Synchrony, Brain Atrophy, and Forgetting. Neuron
642 *97*, 221-230.

643 Hermann, D.M., Siccoli, M., Brugger, P., Wachter, K., Mathis, J., Achermann, P., and Bassetti,
644 C.L. (2008). Evolution of neurological, neuropsychological and sleep-wake disturbances after
645 paramedian thalamic stroke. Stroke; a journal of cerebral circulation *39*, 62-68.

646 Kim, J., Gulati, T., and Ganguly, K. (2019). Competing Roles of Slow Oscillations and Delta
647 Waves in Memory Consolidation versus Forgetting. Cell *179*, 514-526 e513.

648 Kim, J.K., and Fiorillo, C.D. (2017). Theory of optimal balance predicts and explains the amplitude
649 and decay time of synaptic inhibition. Nat Commun *8*, 14566.

650 Klinzing, J.G., Niethard, N., and Born, J. (2019). Mechanisms of systems memory consolidation
651 during sleep. Nature neuroscience *22*, 1598-1610.

652 Krakauer, J.W., Carmichael, S.T., Corbett, D., and Wittenberg, G.F. (2012). Getting
653 neurorehabilitation right: what can be learned from animal models? Neurorehabilitation and neural
654 repair *26*, 923-931.

655 Krueger, J.M., Frank, M.G., Wisor, J.P., and Roy, S. (2016). Sleep function: Toward elucidating
656 an enigma. Sleep Med Rev *28*, 46-54.

657 Latchoumane, C.F.V., Ngo, H.V.V., Born, J., and Shin, H.S. (2017). Thalamic Spindles Promote
658 Memory Formation during Sleep through Triple Phase-Locking of Cortical, Thalamic, and
659 Hippocampal Rhythms. Neuron *95*, 424-435.

660 Macdonell, R.A., Donnan, G.A., Bladin, P.F., Berkovic, S.F., and Wriedt, C.H. (1988). The
661 electroencephalogram and acute ischemic stroke. Distinguishing cortical from lacunar infarction.
662 Archives of neurology *45*, 520-524.

663 Maingret, N., Girardeau, G., Todorova, R., Goutierre, M., and Zugaro, M. (2016). Hippocampo-
664 cortical coupling mediates memory consolidation during sleep. Nature neuroscience *19*, 959-964.

665 Miyamoto, D., Hirai, D., and Murayama, M. (2017). The Roles of Cortical Slow Waves in Synaptic
666 Plasticity and Memory Consolidation. Front Neural Circuits *11*, 92.

667 Navarro-Lobato, I., and Genzel, L. (2019). The up and down of sleep: From molecules to
668 electrophysiology. Neurobiol Learn Mem *160*, 3-10.

669 Ngo, H.-V.V., Miedema, A., Faude, I., Martinetz, T., Mölle, M., and Born, J. (2015). Driving sleep
670 slow oscillations by auditory closed-loop stimulation—a self-limiting process. Journal of
671 Neuroscience *35*, 6630-6638.

672 Ngo, H.V., Martinetz, T., Born, J., and Molle, M. (2013). Auditory closed-loop stimulation of the
673 sleep slow oscillation enhances memory. Neuron *78*, 545-553.

674 Nita, D.A., Cisse, Y., Timofeev, I., and Steriade, M. (2007). Waking-sleep modulation of
675 paroxysmal activities induced by partial cortical deafferentation. Cereb Cortex *17*, 272-283.

676 Norrving, B., and Kissela, B. (2013). The global burden of stroke and need for a continuum of
677 care. Neurology *80*, S5-12.

678 Pack, A.I., Galante, R.J., Maislin, G., Cater, J., Metaxas, D., Lu, S., Zhang, L., Von Smith, R., Kay,
679 T., Lian, J.*, et al.* (2007). Novel method for high-throughput phenotyping of sleep in mice. Physiol
680 Genomics *28*, 232-238.

681 Pearson-Fuhrhop, K.M., Kleim, J.A., and Cramer, S.C. (2009). Brain plasticity and genetic factors.
682 Top Stroke Rehabil *16*, 282-299.

683 Peyrache, A., Battaglia, F.P., and Destexhe, A. (2011). Inhibition recruitment in prefrontal cortex
684 during sleep spindles and gating of hippocampal inputs. Proceedings of the National Academy of
685 Sciences of the United States of America *108*, 17207-17212.

686 Peyrache, A., Khamassi, M., Benchenane, K., Wiener, S.I., and Battaglia, F.P. (2009). Replay of
687 rule-learning related neural patterns in the prefrontal cortex during sleep. Nature neuroscience *12*,
688 919-926.

689 Poryazova, R., Huber, R., Khatami, R., Werth, E., Brugger, P., Barath, K., Baumann, C.R., and
690 Bassetti, C.L. (2015). Topographic sleep EEG changes in the acute and chronic stage of
691 hemispheric stroke. Journal of sleep research *24*, 54-65.

692 Ramanathan, D.S., Gulati, T., and Ganguly, K. (2015). Sleep-Dependent Reactivation of
693 Ensembles in Motor Cortex Promotes Skill Consolidation. PLoS Biol *13*, e1002263.

694 Ramanathan, D.S., Guo, L., Gulati, T., Davidson, G., Hishinuma, A.K., Won, S.J., Knight, R.T.,
695 Chang, E.F., Swanson, R.A., and Ganguly, K. (2018). Low-frequency cortical activity is a
696 neuromodulatory target that tracks recovery after stroke. Nature Medicine *24*, 1257-+.

697 Robinson, M.J., Macrae, I.M., Todd, M., Reid, J.L., and McCulloch, J. (1990). Reduction of local
698 cerebral blood flow to pathological levels by endothelin-1 applied to the middle cerebral artery in
699 the rat. Neurosci Lett *118*, 269-272.

700 Roome, R.B., Bartlett, R.F., Jeffers, M., Xiong, J., Corbett, D., and Vanderluit, J.L. (2014). A
701 reproducible Endothelin-1 model of forelimb motor cortex stroke in the mouse. J Neurosci
702 Methods *233*, 34-44.

703 Sarasso, S., D'Ambrosio, S., Fecchio, M., Casarotto, S., Vigano, A., Landi, C., Mattavelli, G.,
704 Gosseries, O., Quarenghi, M., Laureys, S.*, et al.* (2020). Local sleep-like cortical reactivity in the
705 awake brain after focal injury. Brain : a journal of neurology.

706 Sejnowski, T.J., and Destexhe, A. (2000). Why do we sleep? Brain research *886*, 208-223.

707 Sharkey, J., Ritchie, I.M., and Kelly, P.A. (1993). Perivascular microapplication of endothelin-1: a
708 new model of focal cerebral ischaemia in the rat. J Cereb Blood Flow Metab *13*, 865-871.

709 Siengsukon, C., and Boyd, L.A. (2009a). Sleep enhances off-line spatial and temporal motor
710 learning after stroke. Neurorehabil Neural Repair *23*, 327-335.

711 Siengsukon, C.F., and Boyd, L.A. (2009b). Sleep to learn after stroke: implicit and explicit off-line
712 motor learning. Neurosci Lett *451*, 1-5.

713 Silversmith, D.B., Lemke, S.M., Egert, D., Berke, J.D., and Ganguly, K. (2020). The Degree of
714 Nesting between Spindles and Slow Oscillations Modulates Neural Synchrony. Journal of
715 Neuroscience *40*, 4673-4684.

716 Staresina, B.P., Bergmann, T.O., Bonnefond, M., van der Meij, R., Jensen, O., Deuker, L., Elger,
717 C.E., Axmacher, N., and Fell, J. (2015). Hierarchical nesting of slow oscillations, spindles and
718 ripples in the human hippocampus during sleep. Nature neuroscience *18*, 1679-1686.

719 Steriade, M., McCormick, D.A., and Sejnowski, T.J. (1993). Thalamocortical oscillations in the
720 sleeping and aroused brain. Science *262*, 679-685.

721 Steriade, M., and Timofeev, I. (2003). Neuronal plasticity in thalamocortical networks during sleep
722 and waking oscillations. Neuron *37*, 563-576.

723 Stickgold, R. (2005). Sleep-dependent memory consolidation. Nature *437*, 1272-1278.

724 Tononi, G., and Cirelli, C. (2014). Sleep and the price of plasticity: from synaptic and cellular
725 homeostasis to memory consolidation and integration. Neuron *81*, 12-34.

726 Topolnik, L., Steriade, M., and Timofeev, I. (2003). Partial cortical deafferentation promotes
727 development of paroxysmal activity. Cereb Cortex *13*, 883-893.

728 Tu-Chan, A.P., Natraj, N., Godlove, J., Abrams, G., and Ganguly, K. (2017). Effects of
729 somatosensory electrical stimulation on motor function and cortical oscillations. J Neuroeng
730 Rehabil *14*, 113.

731 van Dellen, E., Hillebrand, A., Douw, L., Heimans, J.J., Reijneveld, J.C., and Stam, C.J. (2013).
732 Local polymorphic delta activity in cortical lesions causes global decreases in functional
733 connectivity. Neuroimage *83*, 524-532.

734 Virley, D., Hadingham, S.J., Roberts, J.C., Farnfield, B., Elliott, H., Whelan, G., Golder, J., David,
735 C., Parsons, A.A., and Hunter, A.J. (2004). A new primate model of focal stroke: endothelin-1-
736 induced middle cerebral artery occlusion and reperfusion in the common marmoset. J Cereb
737 Blood Flow Metab *24*, 24-41.

738 Vock, J., Achermann, P., Bischof, M., Milanova, M., Muller, C., Nirkko, A., Roth, C., and Bassetti,
739 C.L. (2002). Evolution of sleep and sleep EEG after hemispheric stroke. Journal of sleep research
740 *11*, 331-338.

741 Wong, C.C., Ramanathan, D.S., Gulati, T., Won, S.J., and Ganguly, K. (2015). An automated
742 behavioral box to assess forelimb function in rats. J Neurosci Methods *246*, 30-37.

743 Xia, F., Richards, B.A., Tran, M.M., Josselyn, S.A., Takehara-Nishiuchi, K., and Frankland, P.W.
744 (2017). Parvalbumin-positive interneurons mediate neocortical-hippocampal interactions that are
745 necessary for memory consolidation. Elife *6*, e27868.

746 Yang, G., Lai, C.S., Cichon, J., Ma, L., Li, W., and Gan, W.B. (2014). Sleep promotes branch-
747 specific formation of dendritic spines after learning. Science *344*, 1173-1178.

748 Yizhar, O., Fenno, L.E., Prigge, M., Schneider, F., Davidson, T.J., O'Shea, D.J., Sohal, V.S.,
749 Goshen, I., Finkelstein, J., Paz, J.T.*, et al.* (2011). Neocortical excitation/inhibition balance in
750 information processing and social dysfunction. Nature *477*, 171-178.

751

752

Acknowledgements. Research was supported by awards from the Department of Veterans Affairs, Veterans Health Administration (VA Merit: 1I01RX001640 to K.G.; VA CDA to DR, 7IK2BX003308); the National Institute of Neurological Disorders and Stroke (5K02NS093014 to K.G.); and the Basic Science Research Program through the National Research Foundation of Korea (2018R1A6A3A03013031 to J.K.). Karunesh Ganguly, M.D., Ph.D., and Dhakshin Ramanathan, MD., PhD hold a Career Award for Medical Scientists from the Burroughs Wellcome Fund.

Author Contributions. JK, LG, DSR, SW and KG conceived and designed the experiments. JK, LG, AH, SL, and SW conducted the experiments. JK analyzed all data, LG analyzed the data for Fig. 1C, and AH analyzed the data for Fig. 5. JK and KG wrote and edited the manuscript.

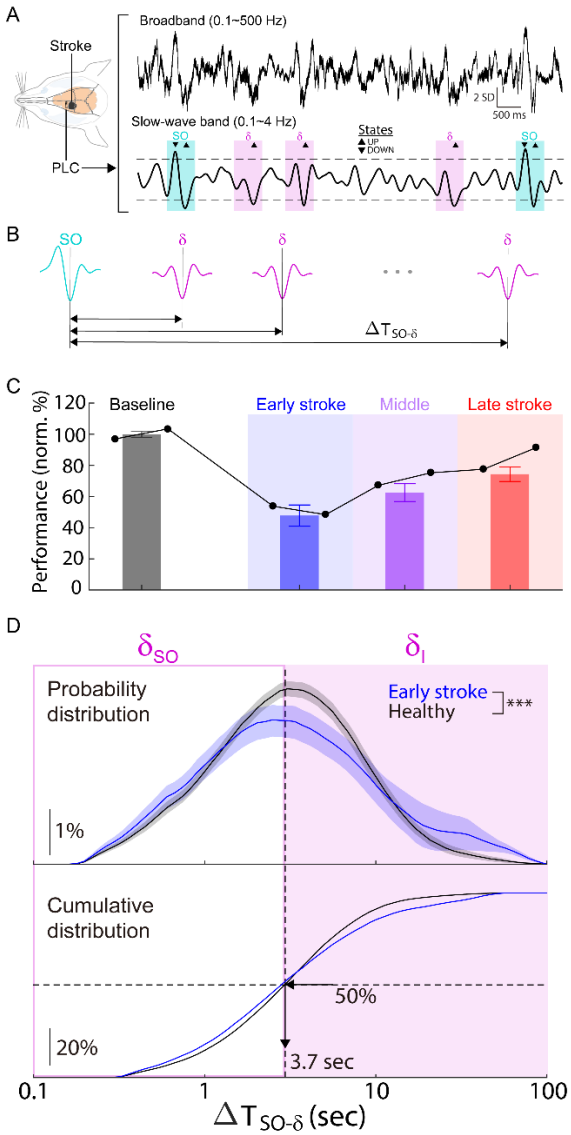

Figure 1. Pathological increase of isolated δ (δ_I) after stroke.
A, Examples of the broadband (0.1-500 Hz) and the filtered (0.1-4 Hz) trace in PLC with stroke. SO and δ-waves are marked by cyan and magenta boxes, respectively.
B, Schematic showing the temporal distance of δ-waves from SO ($\Delta T_{SO\text{-}\delta}$).
C, Mean pellet retrieval success rates (n=8 rats; two sessions per period are shown for a single animal). Bars show average of sessions grouped into tertiles. Mean in vertical bar ± s.e.m. in errorbar. Performance was normalized by the baseline. Stroke impaired motor performance (baseline, n = 16 sessions in 8 rats: 100 ± 1.9% vs. early, n = 16 sessions in 8 rats: 47.8 ± 6.8%; mixed-effects model, $t_{30} = -7.44$, $P < 10^{-7}$). It improved over the subsequent training (late, n = 16 sessions in 8 rats: 75.4 ± 4.7%; early vs. late, mixed-effects model, $t_{30} = 5.78$, $P < 10^{-5}$).
D, Comparison of SO-coupled δ (δ_{SO}) and isolated δ (δ_I) waves for sleep sessions in the early stroke (blue; n = 16 sessions, 8 rats) and sleep sessions in the intact brain of healthy animals. (black; n = 9 sessions, 5 rats; Kolmogorov-Smirnov test, KS-statistic = 0.17, ***$P < 10^{-15}$). Average distributions of $\Delta T_{SO\text{-}\delta}$ are shown. δ_{SO} and δ_I waves were separated by the 50th percentile (3.7 sec, vertical dashed line) from the distribution with healthy animals.

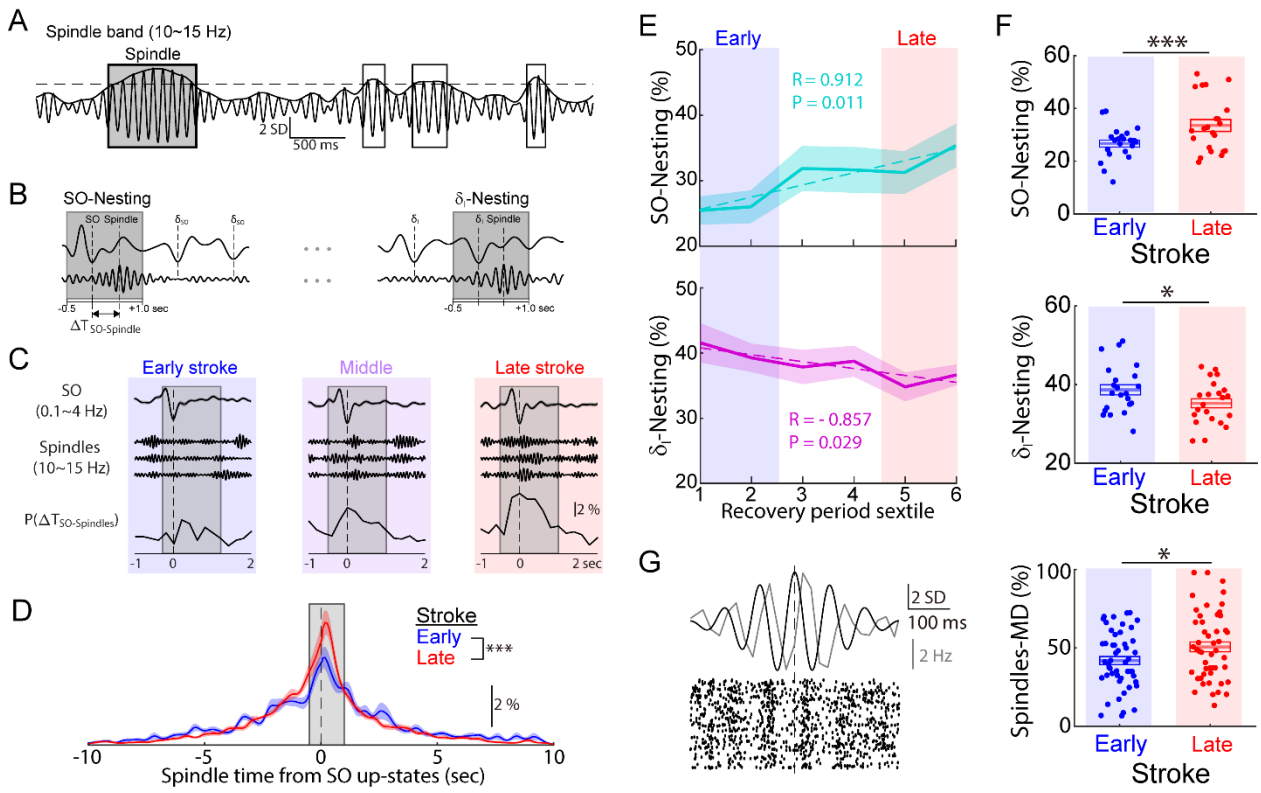

Figure 2. Redistribution of spindles toward SO and the role of δ_I waves.

A, Example LFP trace filtered at spindle band (10-15 Hz) in PLC to detect spindles. Spindles were detected when power exceeded the threshold (1.5sd, horizontal dashed line) for at least 500 ms (filled box). Open boxes show events too brief to be labelled as a spindle.

B, Cartoons of nesting of spindle to SO (SO-Nesting; left) and to δ_I (δ_I-Nesting; right). Gray boxes indicate the time window for 'nesting' which is –0.5 to 1.0 sec from an up-state (same as 'C' and 'D').

C, Examples of SO-spindle temporal interaction in each column of the respective three sessions in "Fig. 1C." Mean SO-up-state-triggered LFP (top, mean ± s.e.m., 0.1~4 Hz). Three single trial examples of detected spindles near a SO (middle). Examples of a probability distribution for the spindle-peaks time from the closest SO up-state, $\Delta T_{SO\text{-}Spindles}$ (bottom). The grey window notes the nesting window.

D, Comparison in distributions of $\Delta T_{SO\text{-}Spindles}$ between the early and late period (n = 22 sessions, 11 rats in each condition; Bartlett's test, $\chi^2 = 58.7$, ***$P < 10^{-13}$).

E, Average time courses of the SO-Nesting and δ_I-Nesting over the recovery period sextile (n = 11 rats). Dashed line represents linear fitting (linear regression; SO-Nesting: R = 0.912, P = 0.011; δ_I-Nesting: R = –0.857, P = 0.029).

F, Comparison of SO-Nesting and δ_I-Nesting between early vs. late period (mean in solid line ± s.e.m. in box; SO-Nesting: early, n = 22 sessions in 11 rats, 26.7 ± 1.3% vs. late, n = 22 sessions in 11 rats, 33.5 ± 2.2%, mixed-effects model, $t_{42} = 3.89$, ***$P < 10^{-3}$; δ_I-Nesting: early, n = 22 sessions in 11 rats, 38.7 ± 1.3% vs. late, n = 22 sessions in 11 rats, 35.2 ± 1.2%, mixed-effects model, $t_{42} = -2.19$, *P = 0.034).

G, Left, average of event-triggered LFP (10~15 Hz; black), spike rates (gray), and raster plot of an example unit; locked to the spindle peaks. Right, modulation-depth of units during spindles for early (n = 50 units, 11 rats; 41.9 ± 3.5%) and late period after stroke (n = 49 units, 11 rats; 50.3 ± 3.7%). There were significant changes from early to late period (mixed-effects model, t_{97} = 2.51, *P = 0.014).

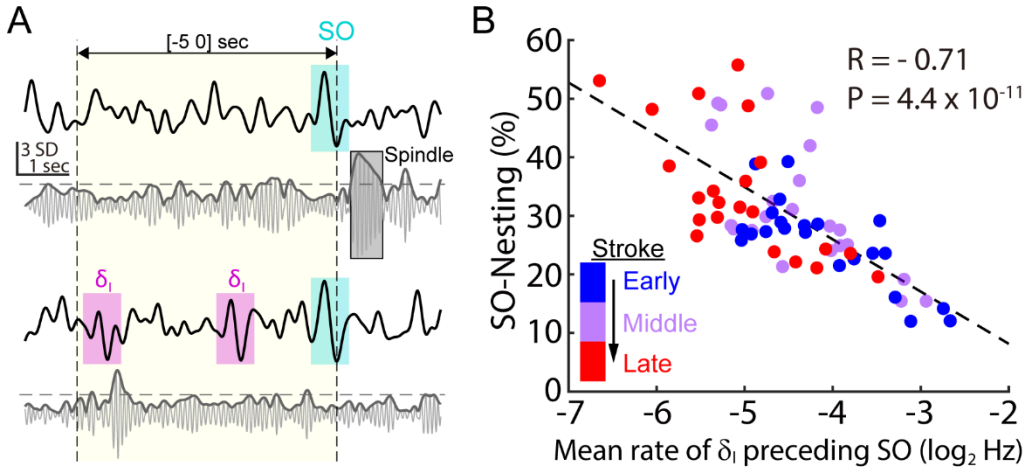

Figure 3. Effect of δ_l-waves preceding SO on SO-spindle nesting.
A, Top, example LFP traces filtered at slow-wave band (0.1-4 Hz; top) and spindle band (10-15 Hz; bottom) in PLC for a case where no δ_l-wave preceded SO during –5-0s from a SO up-state (yellow box). SO, δ_l-waves, and Spindle were detected the same way shown in Figs. 1 and 2. Horizontal dashed line indicates the threshold for detecting spindles. Bottom, same as 'top,' but for a case where two δ_l-waves preceded SO during –5-0s from a SO up-state.
B, Relationship between the mean rate of δ_l-waves preceding SO within 5 sec and the SO-Nesting. There was a negative correlation (dashed line, linear regression, R = –0.71, P = 4.4 x 10^{-11}). This suggests that the prevalence of δ_l-waves directly preceding SO strongly modulates SO-spindle nesting.

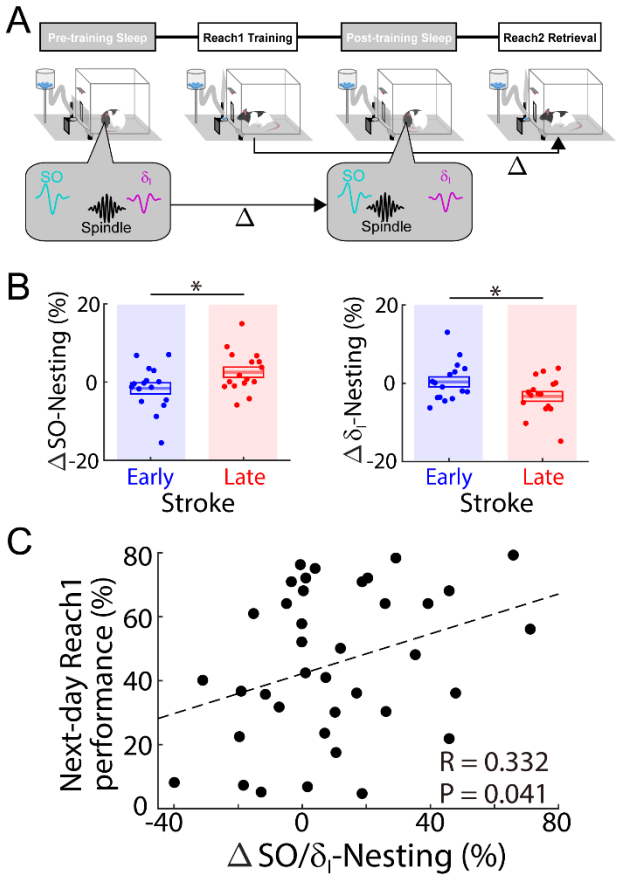

Figure 4. Within-session post rehabilitation changes in spindle redistribution.
A, Flow chart of experiment and schematic results. In a single session, pre-training sleep, training (Reach1), post-training sleep, and retrieval (Reach2) blocks were monitored in sequence.
B, Changes in the SO-Nesting (left) and the δ_l-Nesting (right). ΔSO-Nesting (early, n = 16 sessions in 8 rats, –1.6 ± 1.4% vs. late, n = 16 sessions in 8 rats, 2.6 ± 1.3%, mixed-effects model, t_{30} = 2.24, *P = 0.032). Δδ_l-Nesting (early, n = 16 sessions in 8 rats, 0.3 ± 1.2% vs. late, n = 16 sessions in 8 rats, –3.2 ± 1.2%, mixed-effects model, t_{30} = –2.06, *P = 0.047). Mean in solid line ± s.e.m. in box.
C, Relationship of ΔSO/δ_l-Nesting in 'B' to the next-day reach1 task performance (linear regression, R = 0.332, P = 0.041).

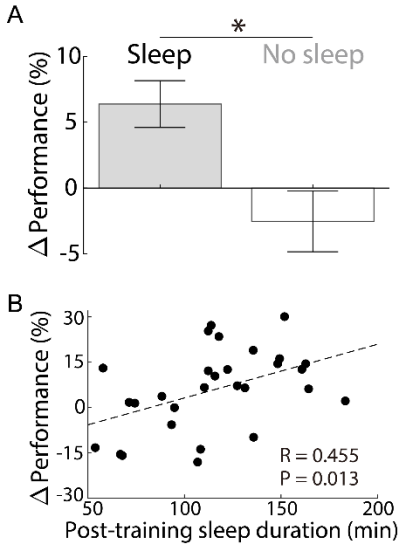

Figure 5. Within-session changes in task performance.
A, Changes in the mean task performance (i.e., pellet retrieval success rate) in each column of the sleep and no-sleep conditions (mean in vertical bar ± s.e.m. in errorbar; sleep: 6.4 ± 1.8%; no-sleep: –2.5 ± 2.3%; sleep vs. no-sleep, two-sample *t*-test, t_{55} = 2.28, P = 0.027).
B, Relationship of the post-training sleep duration (general sleep by video-based detections) to the mean task time change from Reach1 to Reach2 for the sleep group in 'A' (linear regression, R = 0.455, P = 0.013).

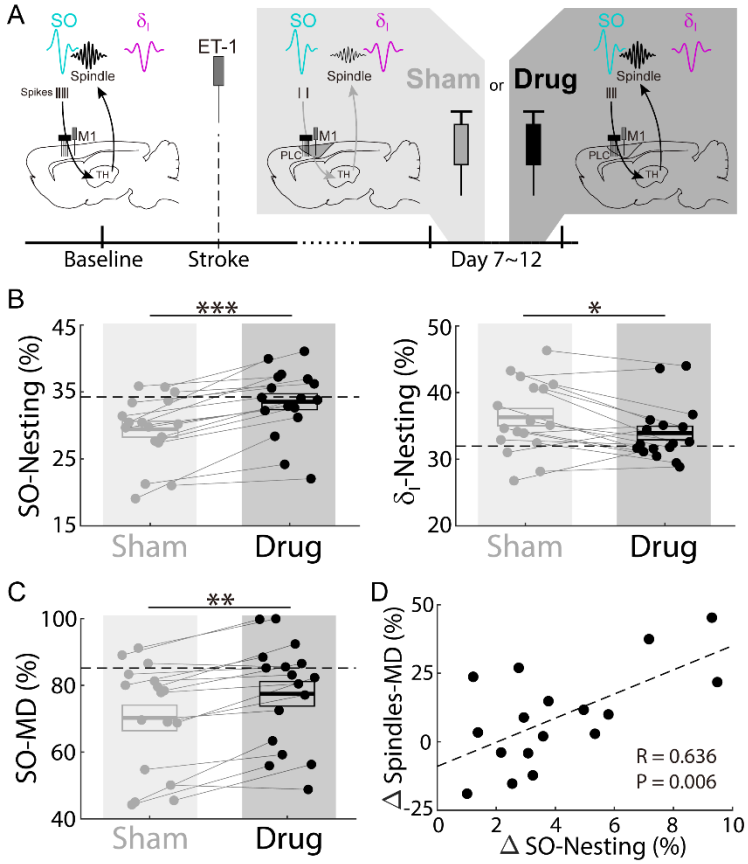

Figure 6. Blocking $GABA_A$ α5-subtype receptor increases SO-Nesting.
A, Flow chart of experiment and schematic results. 32-channel microelectrode arrays with an attached cannula for ET-1 infusion into M1 (n = 3 rats). LFP/spike activity was recorded 2~3 days before inducing ET-1 stroke (vertical dashed line) for the baseline as well as 12 days after the stroke. Either $GABA_A$ α5-subtype receptor inverse agonist (L655-708; drug) or vehicle (saline; sham) was administrated IP on separate days, i.e., range of day 7~12. Stroke resulted in impaired SO-Nesting. Drug enhanced SO-Nesting compared to sham conditions. Same procedural was done for a photothrombotic stroke excluding baseline measurement (n=3 rats). TH: thalamus.
B, Comparison of SO-Nesting and δ_l-Nesting. SO-Nesting and δ_l-Nesting was stronger and weaker, respectively, with the drug compared to the sham (SO-Nesting: sham, n = 17 sessions, 29.4 ± 1.2% vs. drug, n = 17 sessions, 33.5 ± 1.2%, mixed-effects model, $t_{32} = 6.93$, ***$P < 10^{-7}$; δ_l-Nesting: sham, 36.3 ± 1.3% vs. drug, 33.9 ± 1.0%, mixed-effects model, $t_{32} = -2.29$, *P = 0.028). Baseline in horizontal dashed line, mean in solid line ± s.e.m. in box (also in "C").
C, Comparison of unit modulation-depth during SO, i.e., SO-MD; (maximum - minimum) firing rates within –0.5 to 0.3 sec over baseline firing rates within –2 to –0.5 sec from SO up-states. SO-MD was higher with the drug compared to the sham (sham, 70.3 ± 3.8% vs. drug, 77.5 ± 3.7%, mixed-effects model, $t_{32} = 2.79$, **P < 0.01).
D, Relationship from the changes of SO-Nesting in 'B' to the changes of modulation-depth during spindles, i.e., spindles-MD; calculated like SO-MD in 'C' but within –0.25 to 0.15 sec from spindles peaks. There was a positive significant correlation (linear regression, R = 0.636, P = 0.006).

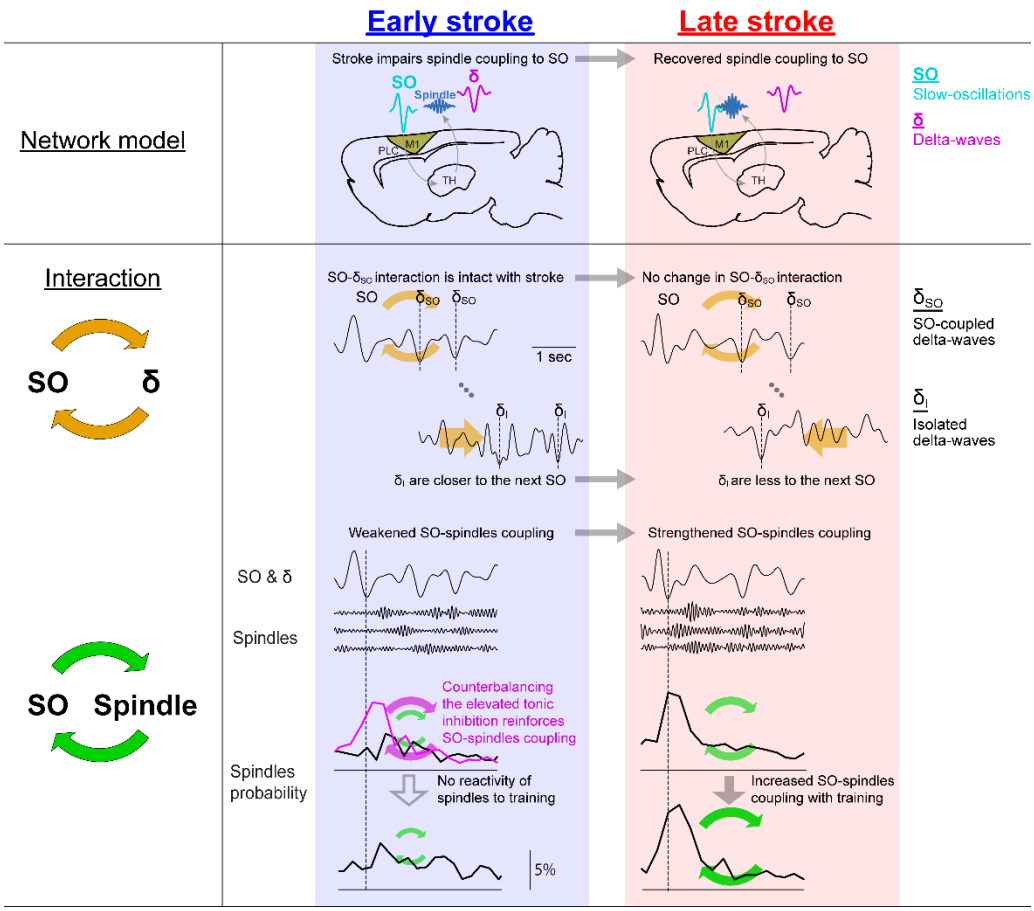

Figure 7. Schematic summary for the proposed model and main results
Stroke likely impairs thalamocortical spindle coupling to SO (blue box, early stroke) and it is more normal with recovery, i.e., precise locking to SO at the late stroke (red box). Interactions between SO and SO-coupled δ-waves (δ_{SO}) is intact after stroke, while δ-waves that are isolated from SO (δ_I) are pathologically redistributed away from SO; pathological δ_I-waves reduces with recovery. SO-spindle coupling is weakened with stroke (early period) and it is normalized with long-term rehabilitation-induced recovery (across-session). Spindles are not reactive to the rehabilitation training (within-session) in early period, i.e., no change in SO-spindle coupling from pre-training sleep to post-training sleep. However, SO-spindle nesting is more reactive to the training with continued recovery. Remarkably, pharmacological treatment to counterbalance the presumed elevated tonic inhibition after stroke may drive memory consolidation and, therefore, enhance SO-spindle coupling associated with functional motor recovery.

885 **SUPPLEMENTARY FIGURES**

886

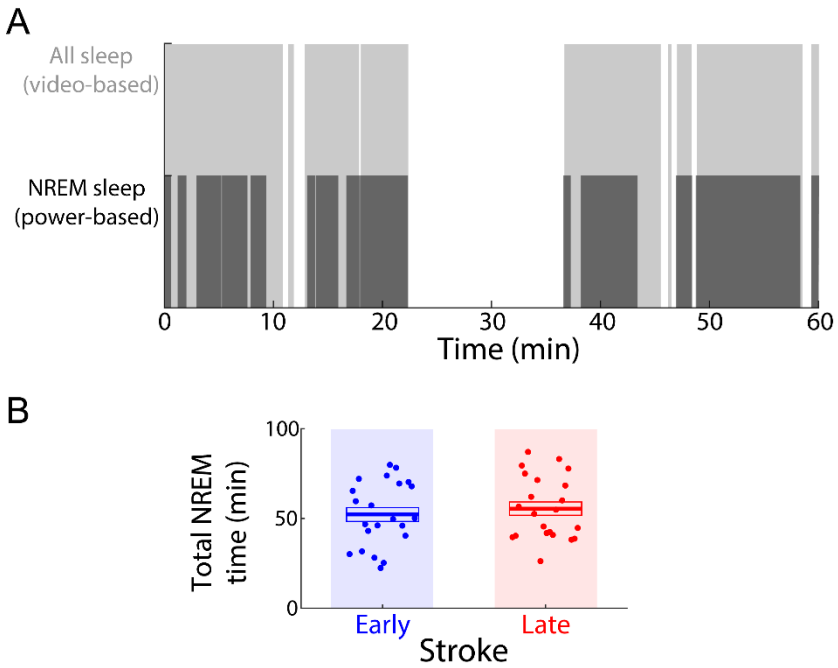

887

888

889 **Supplementary Figure 1. Sleep detection and NREM sleep duration.**
890 **A**, Examples of detections of all sleep using a degree of movement (gray; see Methods) and
891 NREM sleep using power spectral density in 0.1-4 Hz and gamma (30-60 Hz) bands (black).
892 **B**, Mean NREM sleep time during early and late period after stroke. NREM sleep time across all
893 sessions: 52.2 ± 3.9 min during early period (n = 22 sessions in 11 rats), 55.5 ± 3.7 min during
894 late period (n = 22 sessions in 11 rats). No significant difference; early vs. late: mixed-effects
895 model, t_{42} = 0.93, P = 0.36. Mean in solid line ± s.e.m. in box.

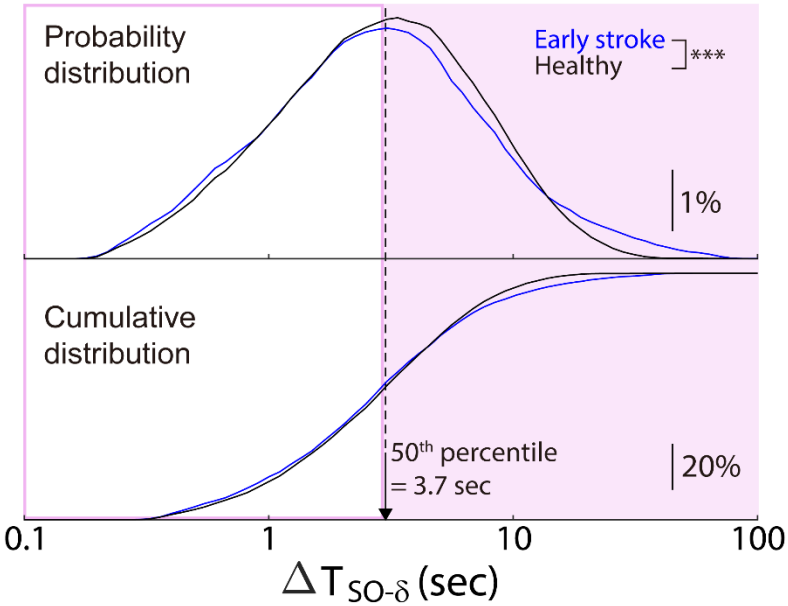

Supplementary Figure 2. Redistribution of δ_l-waves relative to SO after stroke in the same animal.
Example distributions of $\Delta T_{SO\text{-}\delta}$ are shown for sleep sessions in the early stroke (blue; n = 1 rats) and sleep sessions in the intact brain before inducing ET-1 stroke in the same rat. (black; n = 1 rat; Kolmogorov-Smirnov test, KS-statistic = 0.18, ***$P < 10^{-9}$).

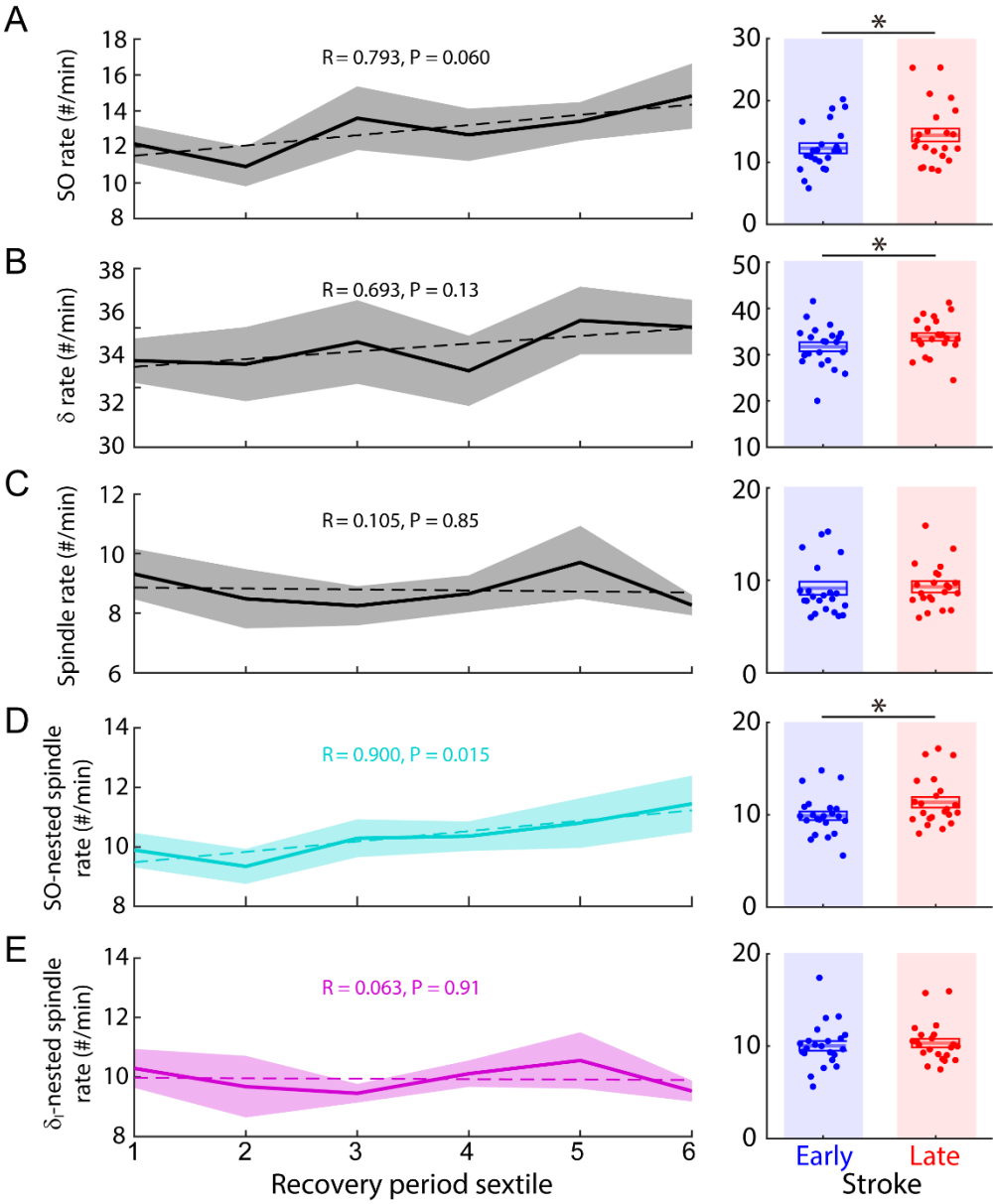

Supplementary Figure 3. Sleep waves rates over the recovery period.
Left, average time courses in the rates of SO (**A**), δ-waves (**B**), spindles (**C**), SO-nested spindles (**D**), and δ_I-nested spindles (**E**) over the recovery period sextile (n = 11 rats). Dashed line represents linear fitting (linear regression; SO: R = 0.793, P = 0.060; δ: R = 0.693, P = 0.13; spindles: R = 0.105, P = 0.85; SO-nested spindles: R = 0.900, P = 0.015; δ_I-nested spindles: R = 0.063, P = 0.91). Right, comparisons between early period and late period in each corresponding metric (early vs. late, mixed-effect model; SO: t_{42} = 2.17, *P = 0.035; δ-waves: t_{42} = 2.56, *P = 0.014; spindles: t_{42} = 0.20, P = 0.85; SO-nested spindle4: t_{42} = 2.15, *P = 0.037; δ_I-nested spindles: t_{42} = 0.50, P = 0.62). Mean in solid line ± s.e.m. in box.

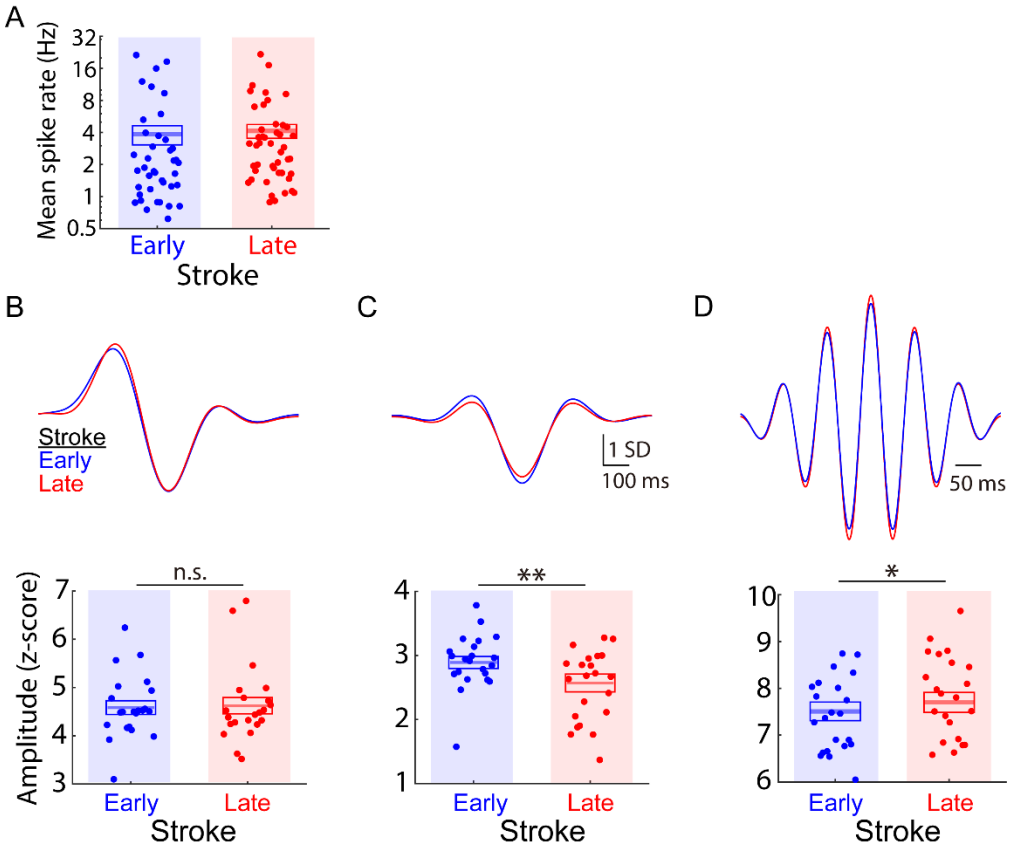

Supplementary Figure 4. Spike activity and Sleep waves amplitude.
A, Mean spike rates of units during NREM sleep for early period and late period after stroke. There was a similar activity for both periods (mixed-effects model, $t_{97} = -0.29$, P = 0.77).
B-D, Top, averages of event-triggered LFPs of SO (**B**), δ_l (**C**), and SO-nested spindles (**D**) for early period (blue; n = 22 sessions, 11 rats) and late period after stroke (red; n = 22 sessions, 11 rats). LFP was normalized; subtracting by the mean and dividing by the standard deviation in each sleep session. Bottom, mean peak-to-trough amplitude corresponding to top. There were significant changes for δ_l and SO-nested spindles from early period to late period (SO: mixed-effects model, $t_{42} = 0.64$, P = 0.53; δ_l: mixed-effects model, $t_{42} = -2.73$, **P < 10^{-2}; SO-nested spindles: mixed-effects model, $t_{42} = 2.51$, *P = 0.016). Mean in solid line ± s.e.m. in box.

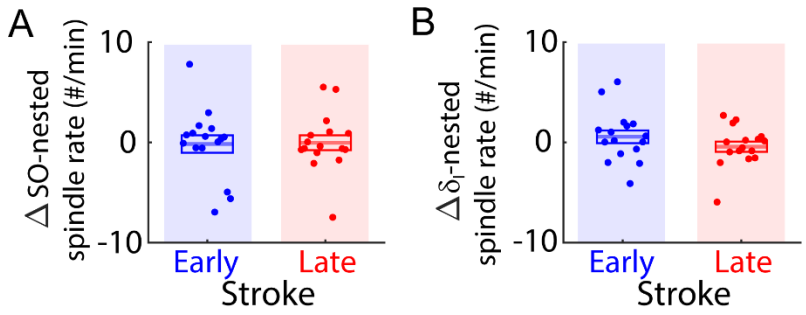

Supplementary Figure 5. Changes in spindles' rates within a single session
Changes of rates in the SO-nested spindles (**A**) and the δ_l-nested spindles (**B**) within a single session (i.e., from pre-training to post-training sleep) in each column of the two stoke periods. ΔSO-nested spindles (early, n = 16 sessions in 8 rats, –0.60 ± 0.45% vs. late, n = 16 sessions in 8 rats, 0.33 ± 0.61%, mixed-effects model, t_{30} = 1.27, P = 0.21). $\Delta\delta_l$-nested spindles (early, n = 16 sessions in 8 rats, 0.56 ± 0.63% vs. late, n = 16 sessions in 8 rats, –0.43 ± 0.50%, mixed-effects model, t_{30} = –1.34, P = 0.19). Mean in solid line ± s.e.m. in box.

	Rat ID	Figs. 1, 2, 3, and 4				Fig. 1	Fig. 6			Fig. 5	
		Stroke animals				Healthy	Stroke animals			Stroke animals	
		Baseline	Early	Middle	Late		Baseline	Sham	Drug	Sleep	No-sleep
Contribution (number of sessions)	1	2†	2	2	2	-	-	-	-	-	-
	2	2†	2	2	2	-	-	-	-	-	-
	3	2†	2	2	2	-	-	-	-	-	-
	4	2†	2	2	2	-	-	-	-	-	-
	5	2†	2	2	2	-	-	-	-	-	-
	6	2†	2	2	2	-	-	-	-	-	-
	7	2†	2	2	2	-	-	-	-	6	-
	8	2†	2	2	2	-	-	-	-	6	-
	9	-	-	-	-	-	-	-	-	8†	-
	10	-	-	-	-	-	-	-	-	6†	-
	11	-	-	-	-	-	-	-	-	5†	-
	12	-	-	-	-	-	-	-	-	4†	-
	13	-	-	-	-	-	-	-	-	-	6†
	14	-	-	-	-	-	-	-	-	-	4†
	15	-	-	-	-	-	-	-	-	-	4†
	16	-	-	-	-	-	-	-	-	-	2†
	17	-	-	-	-	-	-	-	-	-	3†
	18	-	-	-	-	-	-	-	-	-	4†
	19	-	-	-	-	-	-	-	-	-	3†
	20	-	-	-	-	-	-	-	-	-	2†
	21	-	2	2#	2#	2*	2*	3#	3	-	-
	22	-	2	2#	2#	2*	2*	3#	3	-	-
	23	-	2	2#	2#	2*	2*	3#	3	-	-
	24	-	-	-	-	-	-	3	3	-	-
	25	-	-	-	-	-	-	3	3	-	-
	26	-	-	-	-	-	-	2	2	-	-
	27	-	-	-	-	2	-	-	-	-	-
	28	-	-	-	-	1	-	-	-	-	-
	Total	16	22	22	22	9	6	17	17	35	28

Supplementary Table 1. The number of sessions contributed by each rat to the respective experiment types.

All numbers indicate independent contributions to each condition except the numbers marked by star and sharp; * and # indicate the same session that is counted for two conditions. † indicates the sessions in which electrophysiology was not monitored. Rat 21-26 was monitored only for sleep without behavior tasks. Stroke models: photothrombotic for Rat 1-20 and 24-26, and ET-1 induced for Rat 21-23. For behavior data in Fig. 1C, Rat 1-8 were used.

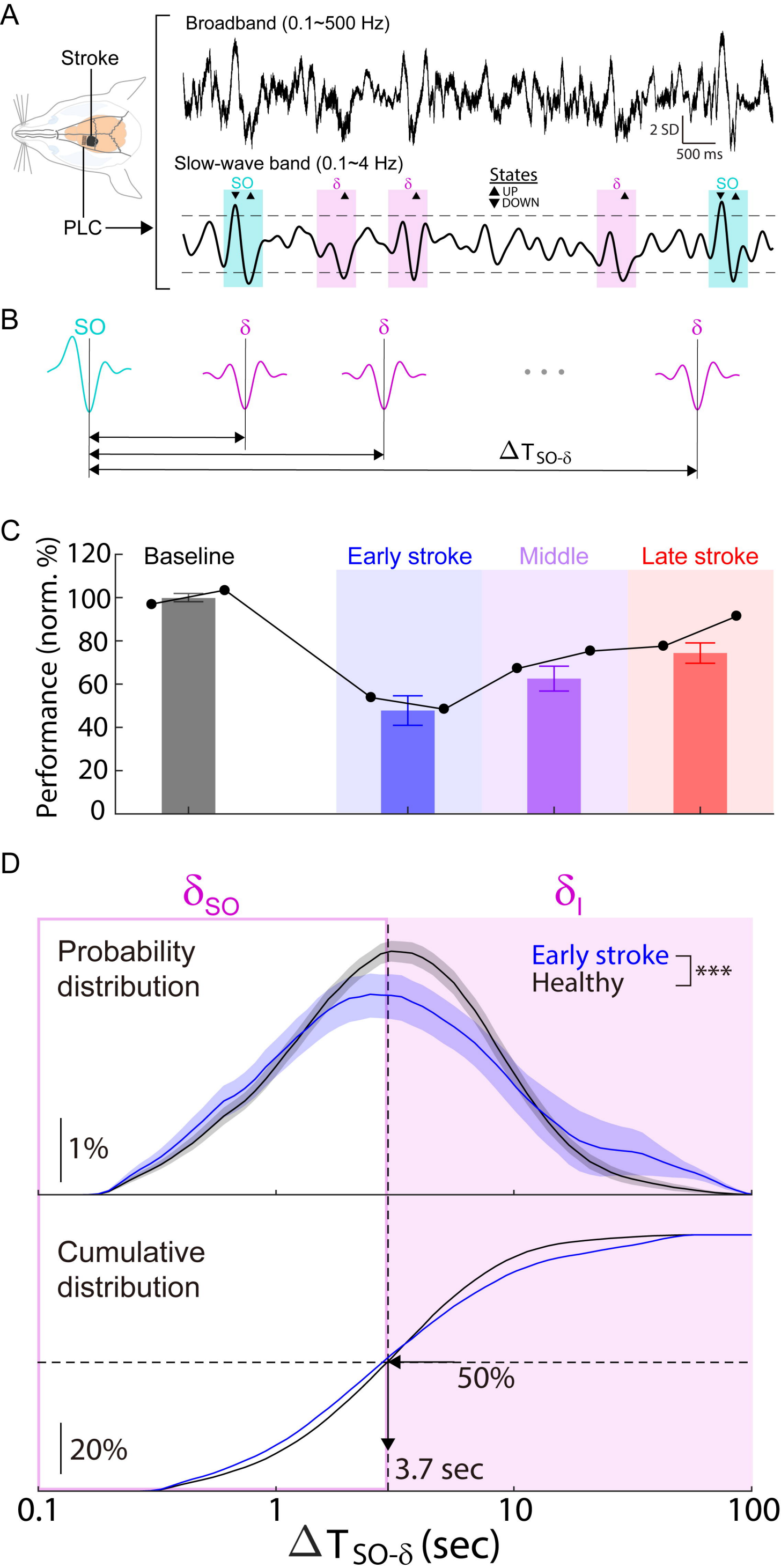
A
Stroke
PLC
Broadband (0.1~500 Hz)
2 SD
500 ms
Slow-wave band (0.1~4 Hz)
SO
δ
States
UP
DOWN
B
SO
δ
ΔT SO-δ
C
Performance (norm. %)
120
100
80
60
40
20
0
Baseline
Early stroke
Middle
Late stroke
D
δSO
δI
Probability distribution
Early stroke
Healthy
***
1%
Cumulative distribution
50%
20%
3.7 sec
0.1
1
10
100
ΔT SO-δ (sec)

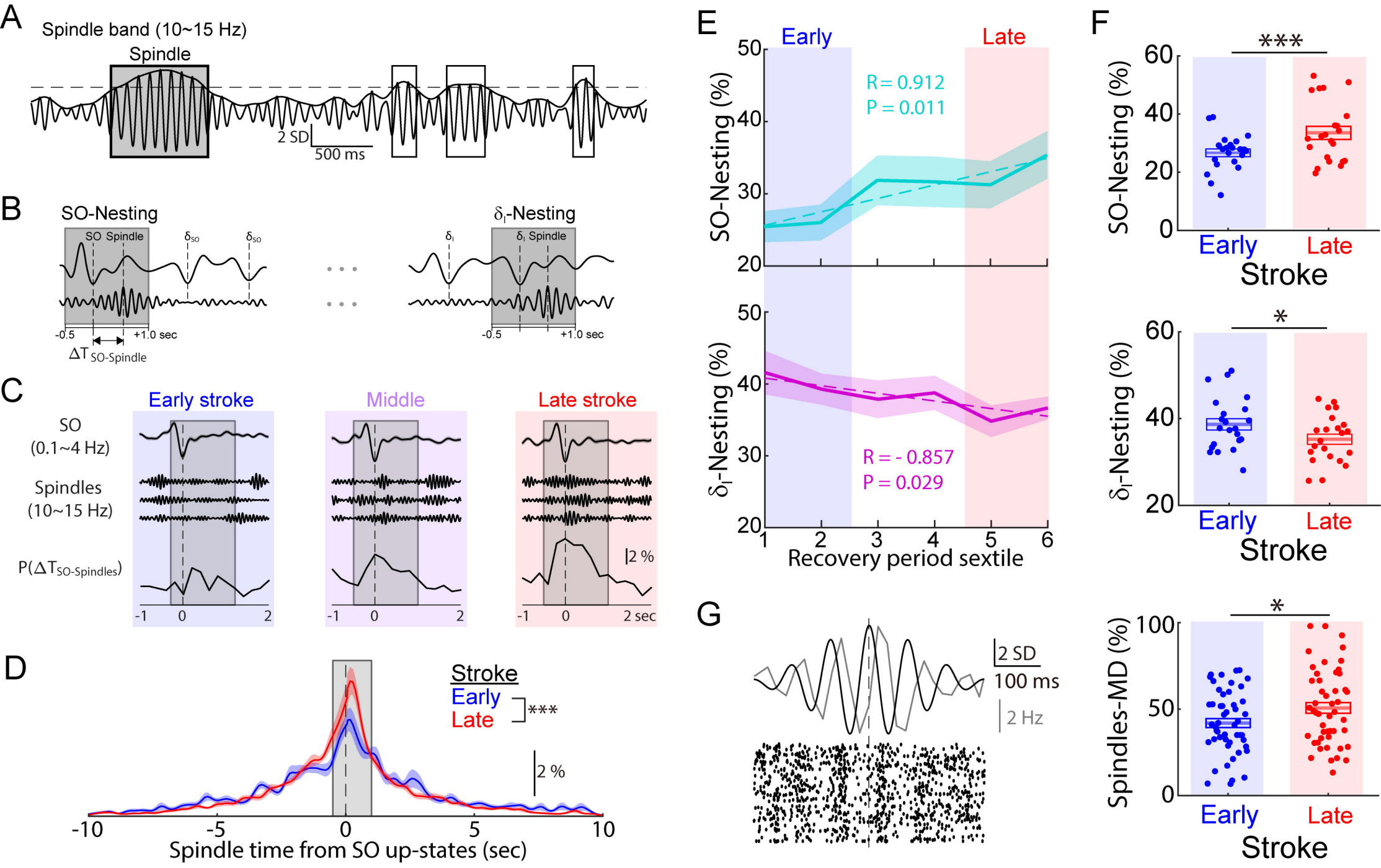
A
Spindle band (10~15 Hz)
Spindle
2 SD
500 ms
B
SO-Nesting
SO Spindle
δSO
δSO
-0.5
+1.0 sec
ΔT SO-Spindle
δI-Nesting
δI
δI Spindle
-0.5
+1.0 sec
C
Early stroke
Middle
Late stroke
SO
(0.1~4 Hz)
Spindles
(10~15 Hz)
P(ΔTSO-Spindles)
2 %
-1
0
2
2 sec
D
Stroke
Early
Late
***
2 %
-10
-5
0
5
10
Spindle time from SO up-states (sec)
E
Early
Late
R = 0.912
P = 0.011
SO-Nesting (%)
R = - 0.857
P = 0.029
δI-Nesting (%)
Recovery period sextile
F
***
SO-Nesting (%)
Early
Late
Stroke
*
δI-Nesting (%)
Early
Late
Stroke
G
2 SD
100 ms
2 Hz
*
Spindles-MD (%)
Early
Late
Stroke

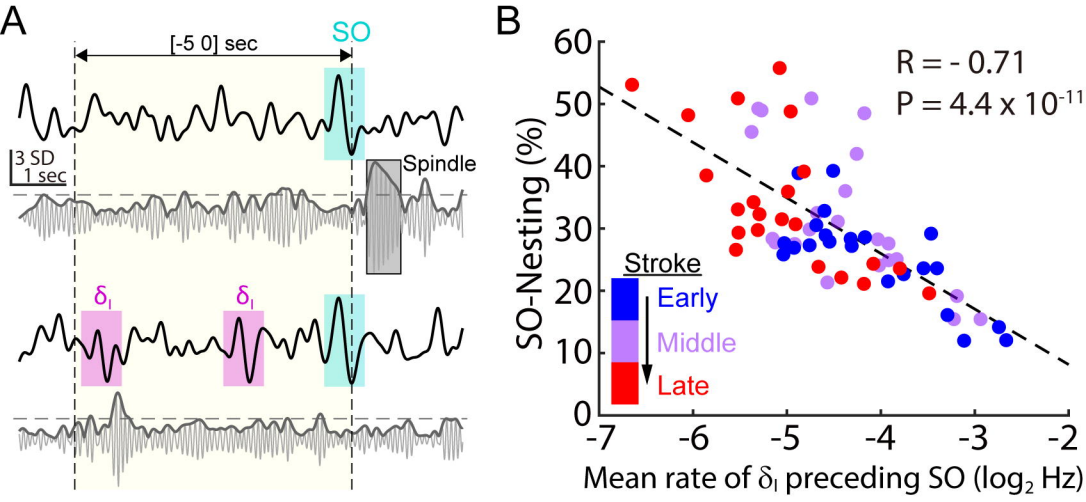
A
[-5 0] sec
SO
3 SD
1 sec
Spindle
δl
δl
B
R = - 0.71
P = 4.4 x 10-11
SO-Nesting (%)
Stroke
Early
Middle
Late
Mean rate of δl preceding SO (log2 Hz)

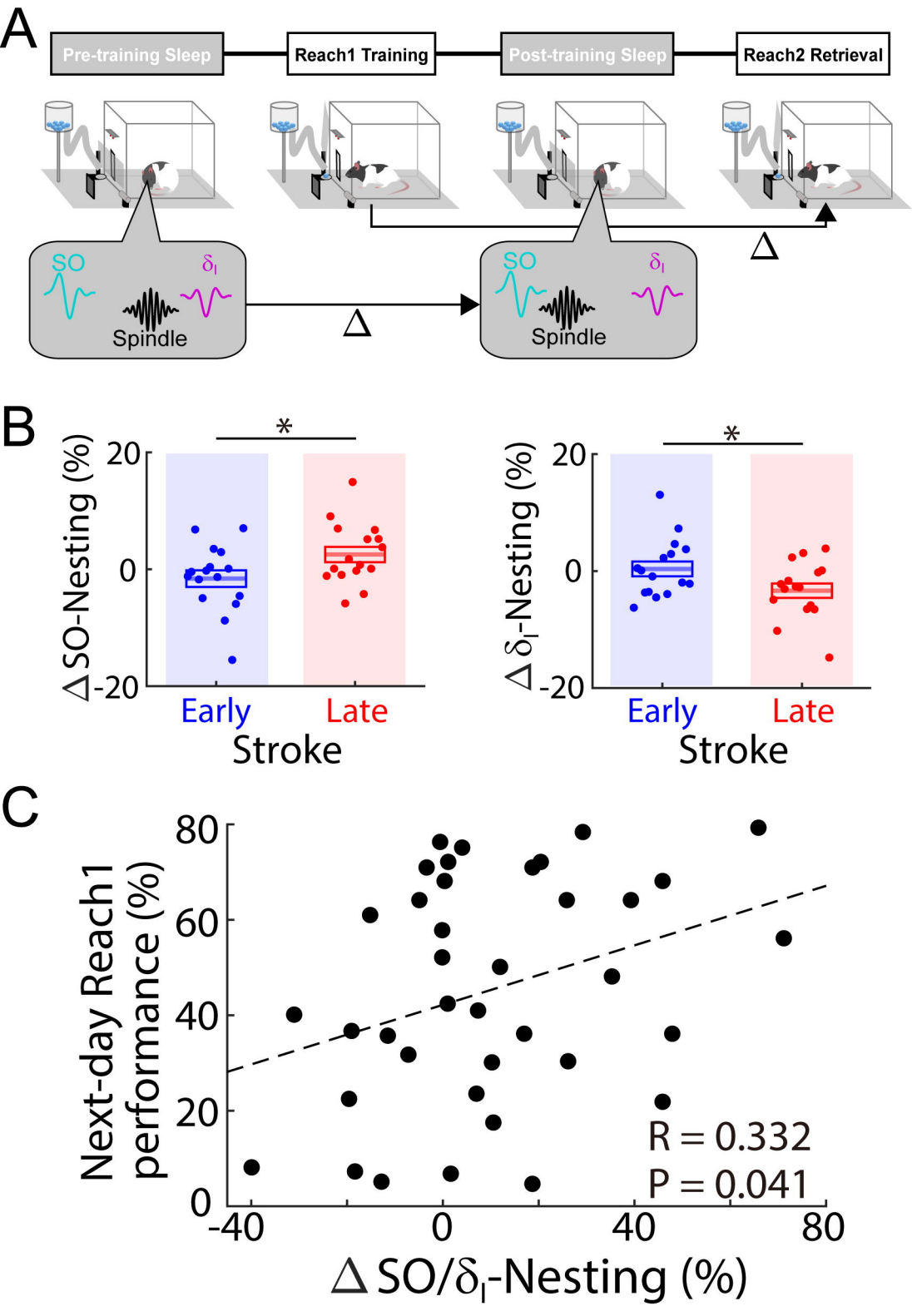
A
Pre-training Sleep
Reach1 Training
Post-training Sleep
Reach2 Retrieval
SO
δl
Spindle
Δ
SO
δl
Spindle
Δ
B
*
20
0
-20
Δ SO-Nesting (%)
Early
Late
Stroke
*
20
0
-20
Δ δl-Nesting (%)
Early
Late
Stroke
C
80
60
40
20
0
Next-day Reach1 performance (%)
R = 0.332
P = 0.041
-40
0
40
80
Δ SO/δl-Nesting (%)

A

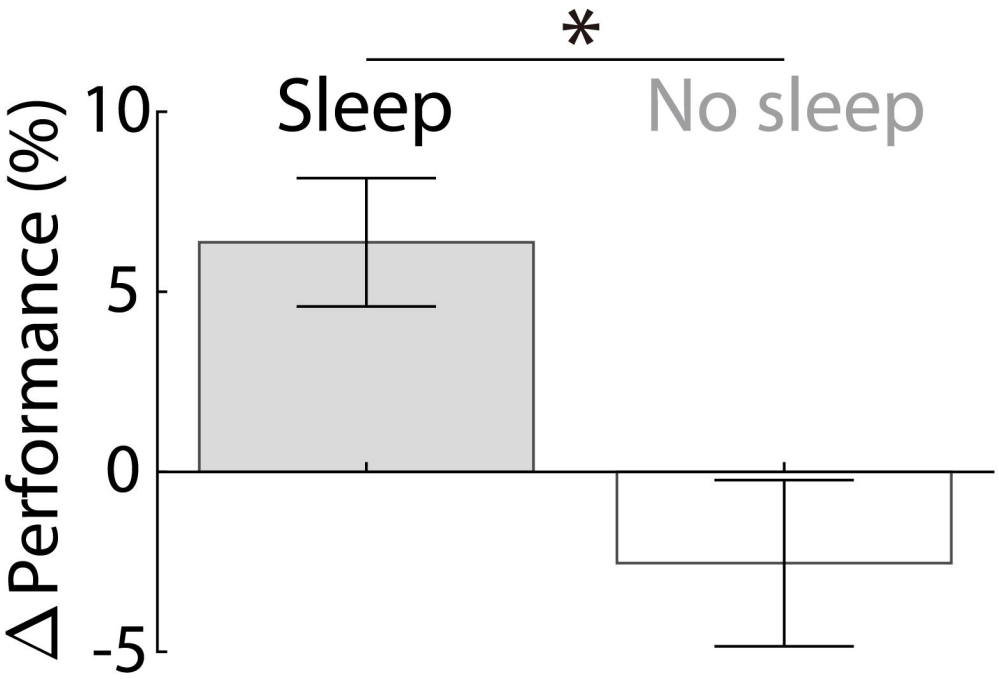
*
Sleep
No sleep
10
5
0
-5
Δ Performance (%)

B

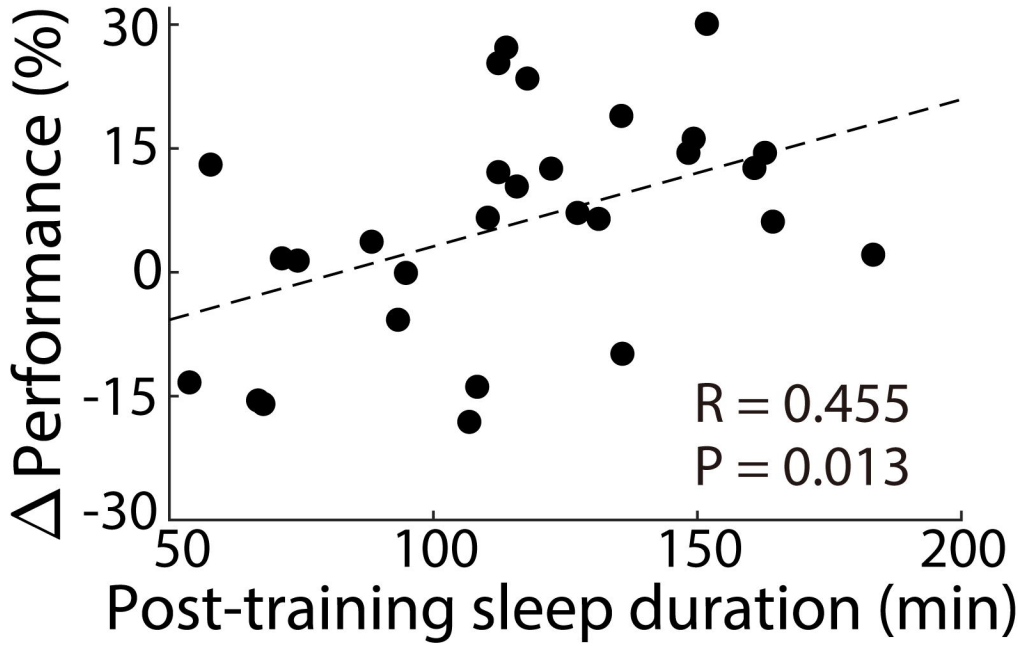
30
15
0
-15
-30
Δ Performance (%)
R = 0.455
P = 0.013
50
100
150
200
Post-training sleep duration (min)

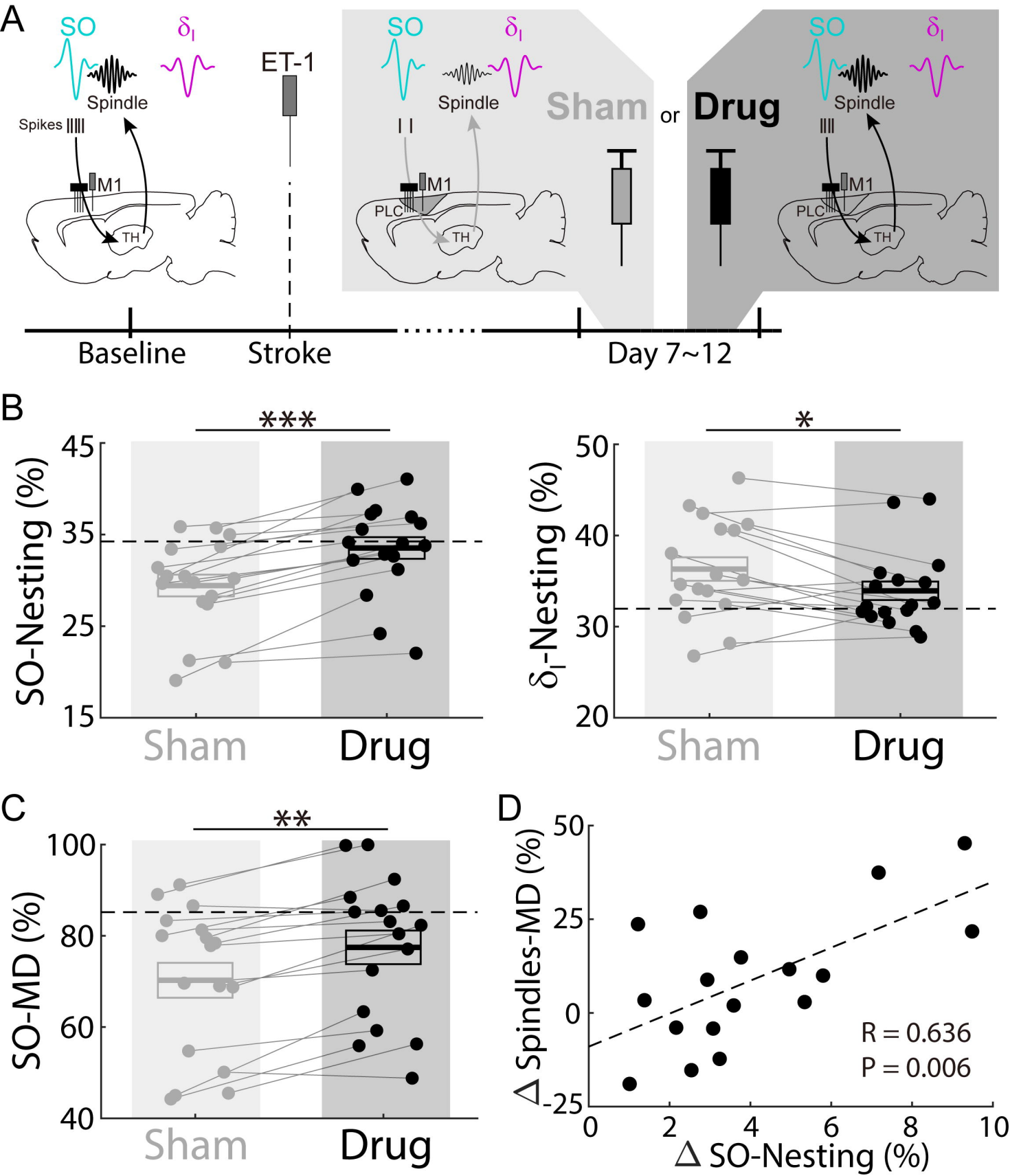
A
SO
δl
Spindle
Spikes
M1
TH
ET-1
Sham
or
Drug
PLC
Baseline
Stroke
Day 7~12
B
***
SO-Nesting (%)
45
35
25
15
Sham
Drug
*
δl-Nesting (%)
50
40
30
20
C
**
SO-MD (%)
100
80
60
40
D
Δ Spindles-MD (%)
50
25
0
-25
R = 0.636
P = 0.006
Δ SO-Nesting (%)
0
2
4
6
8
10

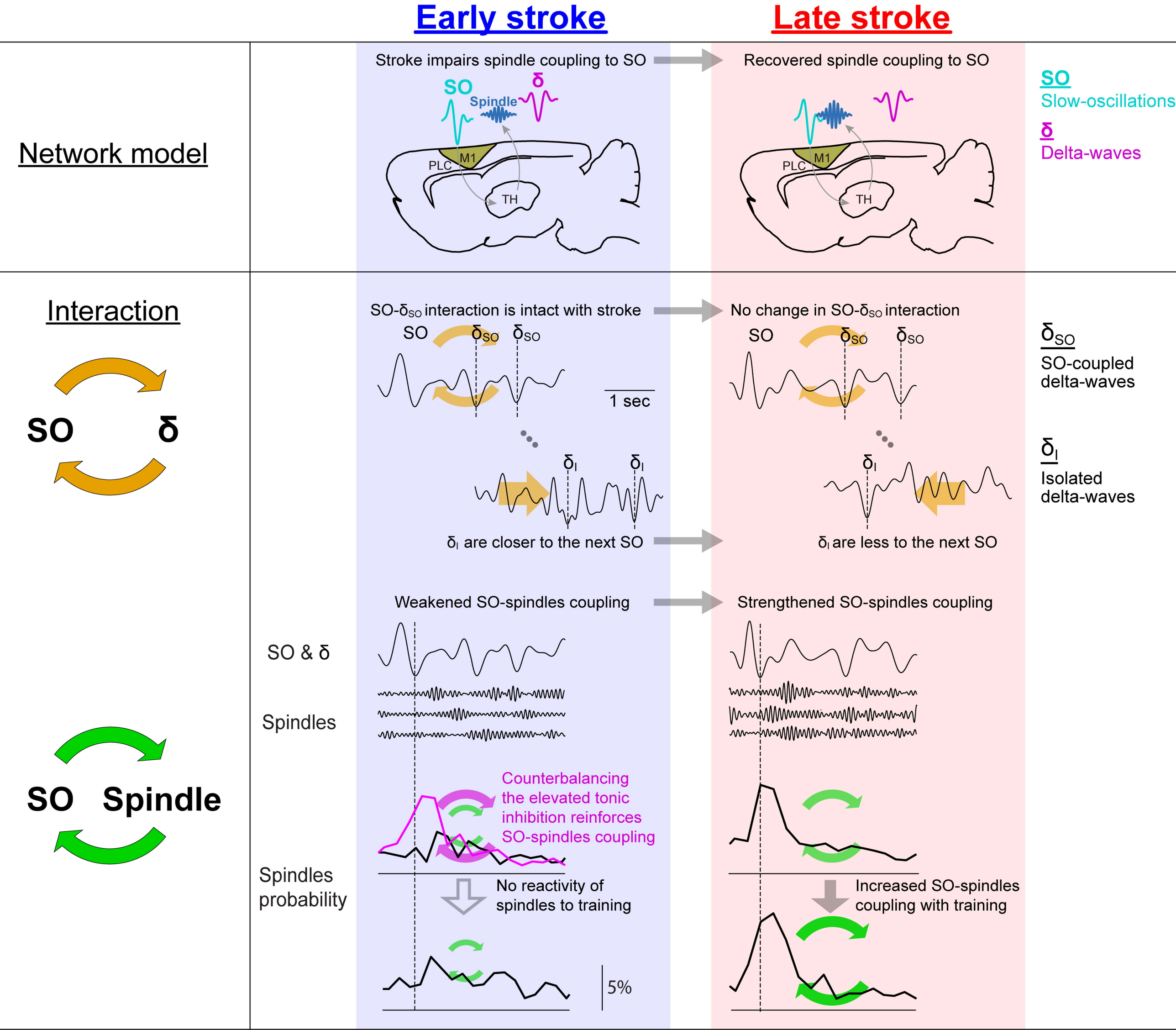
Early stroke
Late stroke
Network model
Stroke impairs spindle coupling to SO
Recovered spindle coupling to SO
SO
Spindle
δ
M1
PLC
TH
SO
Slow-oscillations
δ
Delta-waves
Interaction
SO
δ
SO-δSO interaction is intact with stroke
No change in SO-δSO interaction
SO
δSO
δSO
1 sec
δI
δI are closer to the next SO
δI are less to the next SO
δSO
SO-coupled delta-waves
δI
Isolated delta-waves
SO
Spindle
Weakened SO-spindles coupling
Strengthened SO-spindles coupling
SO & δ
Spindles
Counterbalancing the elevated tonic inhibition reinforces SO-spindles coupling
Spindles probability
No reactivity of spindles to training
Increased SO-spindles coupling with training
5%